THE UNIVERSITY OF MICHIGAN
DEPARTMENT OF ATMOSPHERIC, OCEANIC, AND SPACE SCIENCE

Space Physics Research Laboratory
2245 Hayward Street
Ann Arbor, Michigan 48109-2143

Contract/Grant No.:	NAG5-230
Project Name:	Nitric Acid Oxide Mixing Ratio Measurements Using a Rocket Launched Chemiluminescent Instrument
Report Author(s):	Jack J. Horvath
Author(s) Phone:	313/764-6579
Report Preparation Date:	January 1989
Report Type:	Final Technical Report
Period Covered:	September 1986 through October 1987
Project Director:	Jack J. Horvath
Principal Investigator(s):	no others
Program Technical Officer:	James Margitan
Address:	Code EE Mailstop 85 NASA Headquarters Washington, D.C. 20546

I. INTRODUCTION

A total of eighteen rocket launched-parachute borne nitric oxide instruments were launched for the calendar years 1977 thru 1985. All of these payloads were fabricated before the calendar year 1980. There has been an iteration in the technology as the learning curve progressed but the basic implementation of the experiment has remained unchanged. No changes have been made in the main body of the instruments, i.e., things associated with the reaction volume. Two of these instruments have accounted for twelve of the eighteen launches. And, it is very important to note, the original sensitivity calibration for these instruments remained unchanged over the entire time period. A scale diagram of the flight instrument can be found in Figure 1.

Only six launches were carried out during time period of the current NASA grant. However all of the retrieved data sets have been included here for completeness.

The instrument design was very much a success. It turned out to be a very precise instrument for the measurement of the nitric oxide mixing ratio. Except for the last four rocket launches, however, it did not yield the required absolute values that we hoped for. We encountered two major problems. First, our inappropriate choice of the background calibration gas, nitrogen, caused the first ten data sets to be too low in the absolute mixing ratio by something on the order of 2-5 PPBV. We finally realized the error and substituted air for the bias gas measurement. It should be pointed out that even though our background measurement was in error, giving a systematic offset, the instrument precision was not affected. We will show two comparison data sets which demonstrate the small scale repeatability between payloads that were launched within a time scale on the order of one hour.

Secondly, in our desire to extend the measurement to higher altitudes we ran into the problem of contaminating the inlet flow tube with ozone from the reagent gas, i.e., we opened the ozone valve too early in the flight and this caused the pressure in the reaction volume to exceed the pressure at the flow tube entrance which then permitted zone to migrate backward into the inlet flow tube. Where we did have this kind of a problem the effect was restricted to an altitude above 45 km.

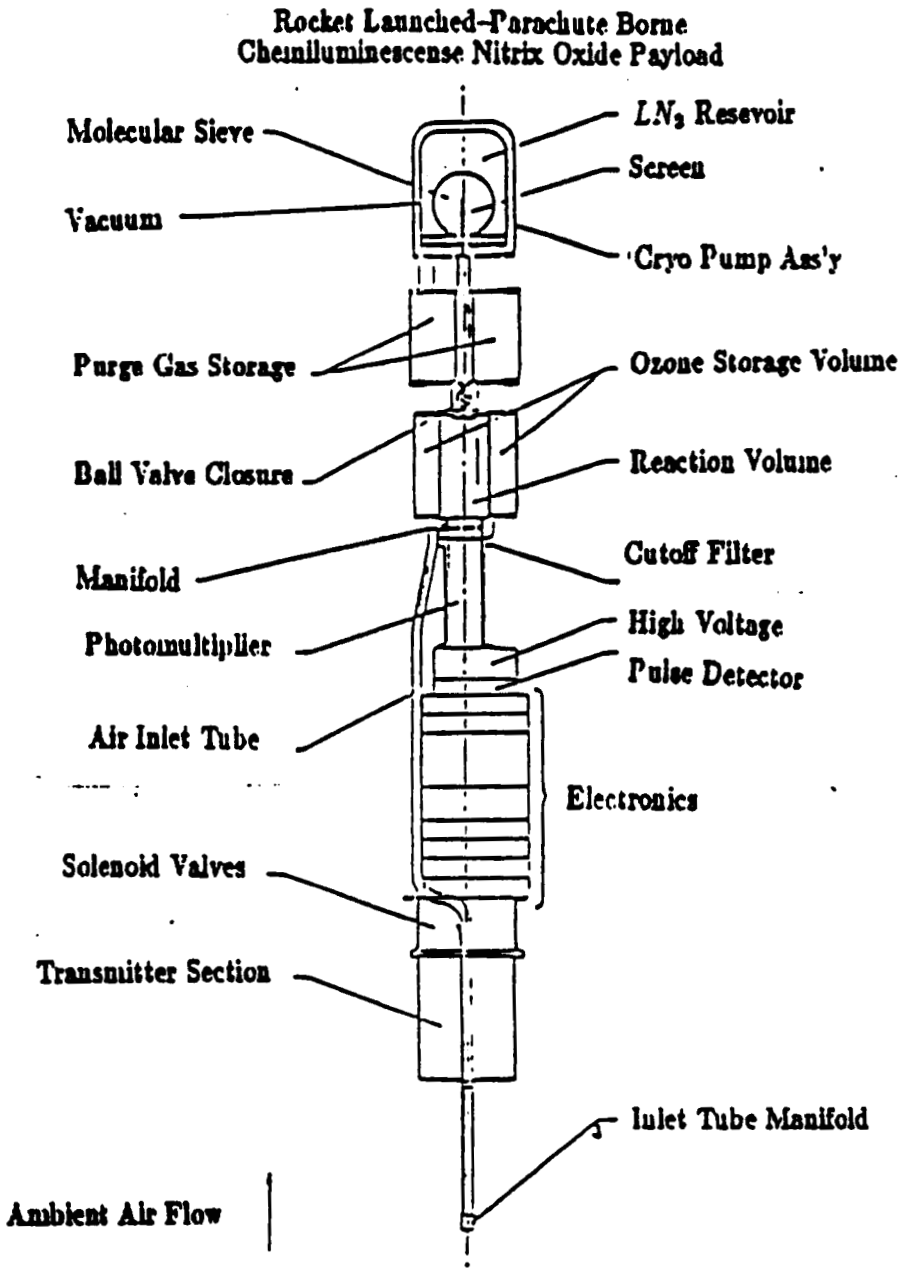

Figure (1) Scale diagram of the rocket launched- parachute borne nitric oxide chemiluminescence payload (M-NORP). The instrument is shown in the orientation it sees during parachute descent.

II. THEORETICAL REVIEW

The first reported evidence of a bimolecular reaction between nitric oxide and ozone was made by Johnson and Crosby [1954]. The resulting chemiluminescence was not observed until Greaves and Garvin reported in 1959 that such emission was due to electronically excited NO_2. Subsequently Clyne, Thrush, and Wayne[1964] proposed the following reaction mechanism:

$$NO + O_3 \rightarrow NO_2^* + O_2 \quad (1)$$

$$\rightarrow NO_2 + O_2 \quad (2)$$

$$NO_2^* \rightarrow NO_2 + h_\nu \quad (3)$$

$$NO_2^* + M_i \rightarrow NO_2 + M_i \quad (4)$$

The operation of a chemiluminescent 'NO' detector is based upon the detection of light emitted by the electronically excited NO_2 molecules which are formed in the reaction between NO and O_3. Reaction (2) competes with (1) and is, in fact, the dominate process. The excited molecules from reaction (1) undergo subsequent de-excitation by either photoemission or collisional de-excitation as per equations (3) and (4) repectively. Clough and Thrush[1967] reported the radiation was spread over the approximate wavelength interval 600 through 3000 nanometers (figure 2).

If only the above four equations are considered, the number of photons generated per second per unit time is given by

$$I = \frac{k_1 k_2 [NO][O_3]}{k_3 + \Sigma_i k_4 [M_i]} \quad (5)$$

where k_1, k_2, k_3, and k_4 are rate constants corresponding to the reaction (1) through (4) and where k_4 is the constant for collisional de-excitation of the ith species.

If ozone is present in excess, i.e., $[O_3] >> [NO]$, then reactions (1) and (2) become first order with respect to nitric oxide and the concentration as a function of time is given by

$$[NO] = [NO]_{t=o} exp\{-(k_1 + k_2)[O_3]t\} \quad /cc \quad (5a)$$

Now, following the development of Mason[1973], if the reaction volume is defined as a plug-flow reactor (figure 3) with the reactant gases entering continuously at one end, the temporal distribution above corresponds to spacial distribution of nitric oxide along the axis of the reactor given by

$$[NO] = [NO]_{z=o} exp\{-(k_1 + k_2)[O_3]Az/Q\} \quad /cc \quad (6)$$

where A is the cross-sectional area of the reactor, Q is the total volume flow, and z is the axial distance from the entrance plane.

Combining equations (5) and (6), the total number of photons emitted per second between z and z+dz is given by

$$I_Z dz = \left[\frac{k_1 k_3 [NO]_o [O_3]}{(k_1 + k_2)(k_3 + \Sigma_i k_4 [M_i])} exp\{-(k_1 + k_2)[O_3]Az/Q\}\right] dz \quad photons/sec \qquad (7)$$

The total volume emission rate, I_V, is obtained by integrating equation (7) over the length of the reaction vessel, i.e.,

$$I_V = \frac{k_1 k_3 [NO]_o Q}{(k_1 + k_2)(k_3 + \Sigma_i k_4 [M_i])} \{1 - exp\{-(k_1 + k_2)[O_3]AZ/Q\}\} \quad photons/sec \qquad (8)$$

where Z is the physical length of the cylindrical chamber. The temperature dependent rate constants for equations (1) and (2) as given by Clough and Thrush[1967] are

$$k_1 = 1.26(10)^{-12} exp(-2090/T) \quad cc/sec$$

$$k_2 = 7.14(10)^{-13} exp(-1165/T) \quad cc/sec$$

and their interpretation of the rate constants k_3 and k_4, for oxygen, lead to a ratio

$$k_4/k_3 = 2.7(10)^{14} \quad /cc.$$

To the extent that k_4 can be assumed independent upon species the denominator in equation (8) can be written as

$$(k_1 + k_2)(k_3 + k_4 \Sigma_i [M_i]) = (k_1 + k_2)(k_3 + k_4 P_C/kT)$$

with $[M_i]$ proportional to the total pressure in the reaction volume. Also, $[NO]_o Q$ is simply the 'NO' flux(molcules/sec.) into the reactor which can be expressed as

$$[NO]_o Q = F_{(air)} \Omega_{(NO)} P_o / kT_o$$

Thus equation (8) can be rewritten to give

$$I_V = \frac{k_1 P_o F_{(air)} \Omega_{(NO)}}{(k_1 + k_2) kT_o (1 + k_4 P_C / k_3 kT)} \{1 - exp\{-(k_1 + k_2)[O_3]AZ/Q\}\} \quad photons/sec \qquad (9)$$

where the units of pressure, P_C, are give in Torr., temperature, T, is given in degrees Kelvin, k is Boltzmann's constant, and F_{air} is the volume flow rate of the incomming gas sample in cc./second @ N.T.P. with an 'NO' mixing ratio $\Omega(NO)$. The distribution of photons in the reaction volume is governed by the reaction length

$$L = \frac{Q}{(k_1 + k_2)[O_3]A} \quad cm. \tag{10}$$

The ozone concentration in the reaction volume is represented by

$$[O_3] = \frac{P_C \Omega_{(O_3)} F_{O_3}}{kT(F_{(air)} + F_{O_3})} \quad /cc$$

and the total volume flow rate refered to NTP is

$$Q = \frac{(F_{air} + F_{O_3})P_o T}{P_C T_o}$$

to give a theoretical measure of the reaction length in terms of instrument related parameters, i.e.,

$$L = \frac{(F_{(air)} + F_{(O_3)})^2 T k P_o}{(k_1 + k_2) P_C{}^2 F_{(O_3)} \Omega_{(O_3)} A T_o} \quad cm \tag{11}$$

where $F_{(O_3)}$ is the reagent gas flow(ozone in a mixture with oxygen)with the units cc./seconds @ N.T.P., and $\Omega_{(O_3)}$ is the ozone mixing ratio of the reagent gas as it resides in the storage resevoir.

Thus, for a given cylindrical reaction volume where the reactant gases, $F_{(air)}$ and $F_{(O_3)}$, enter continuously at one end equations (9) and (11) can be used to predict the total possible photon production per unit time.

It is important to realize that all of the photons, generated within the reaction vessel, are not detected. In fact, only a small fraction contribute to produce an 'NO' signal. Two major loss mechanisms are present. First, since photons are generated throughout the reaction volume in a manner proportional to the exponential decay of nitric oxide and since, to first order, the probability of any one particular photon arriving at the detector depends upon solid angle geometry, the probability of observing photons is quite sensitive to reaction length. Therefore, the relation between the number photons produced and the number intercepted must be some function of reaction length. This function, a variable, is defined as $G(L)$.

Secondly, the emission spectrum begins in the near infrared- (figure 2) which requires that the photomultiplier tube selection be a compromise between adequate spectral response over some fraction of the $NO - O_3$ response curve and a resonably low 'dark' count signal, I_B. A relative response function can be defined as the product of the photomultiplier tube quantum efficiency, $E(\lambda)$, and the relative intensity of the chemiluminescent emission spectra, $I(\lambda)$. If the response function is integrated with respect to wavelength and devided by the total possible quanta, the result can be defined as the effective quantum yield which is a measure of the number of photons that yield one(1) photoelectron, i.e.,

$$Y = \frac{\int_o^\infty E(\lambda)I(\lambda)d\lambda}{\int_o^\infty I(\lambda)d\lambda}. \tag{12}$$

The effective quantum yield together with a corresponding evaluation of I_B is a basis for selection of photomultiplier tubes.

If the two loss mechanisms, above, are considered, equation 9 (which computes the total photon production) can be modified to give an emperical expression

$$I_S = \frac{k_1 P_o F_{(air)} \Omega_{(NO)} Y G(L)}{(k_1 + k_2) k T_o \{1 + (k_4/k_3)(P_C/kT)\}} \quad photons/sec \tag{13}$$

where I_S is the actual output counting rate for a given set of flow conditions.

Equations (13) and (11) are general expressions which form a mathematical model for any chemiluminescent nitric oxide detection system using cylindrical geometry.

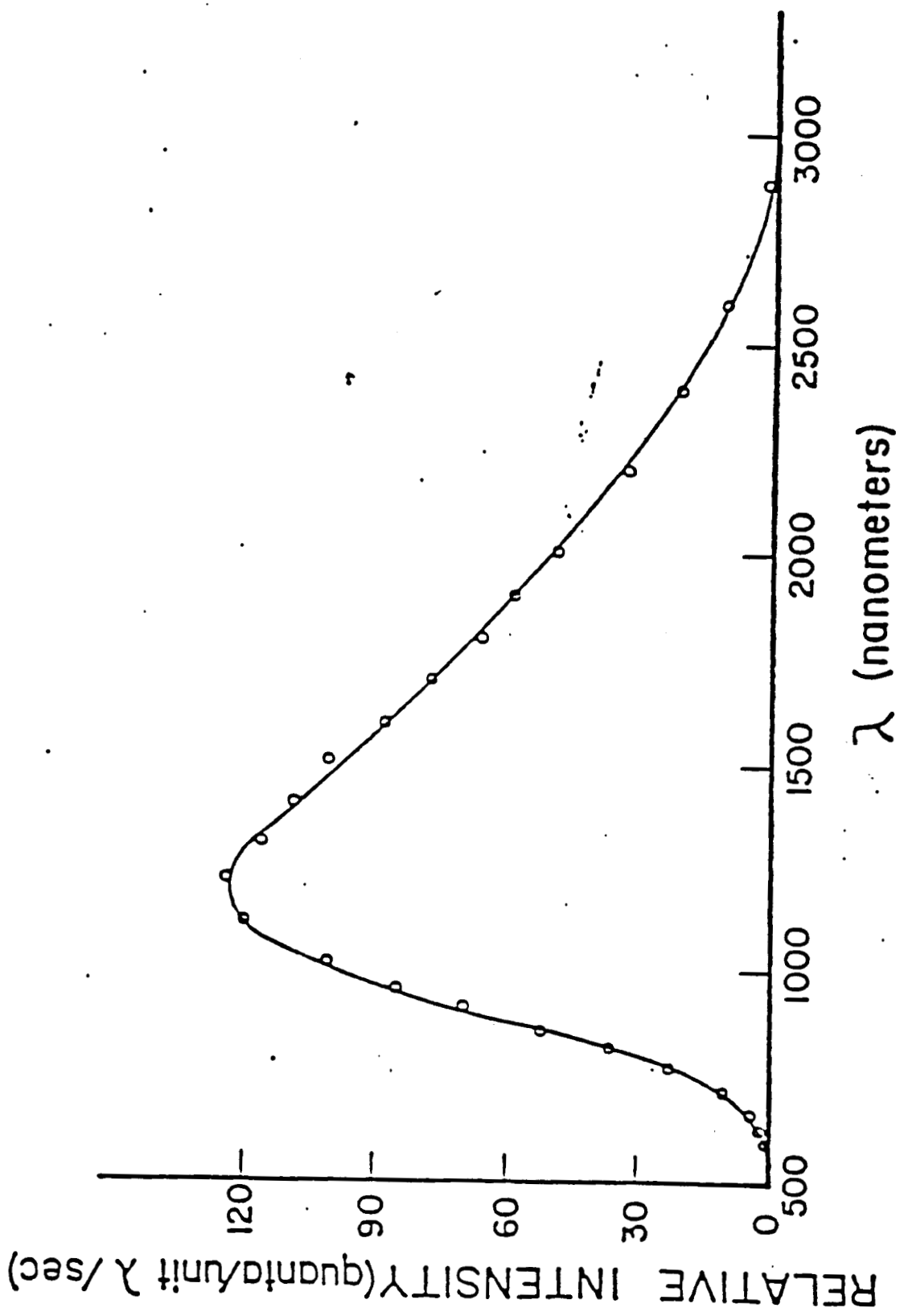

Figure (2) Emission spectrum for NO-O_3) chemiluminescence.

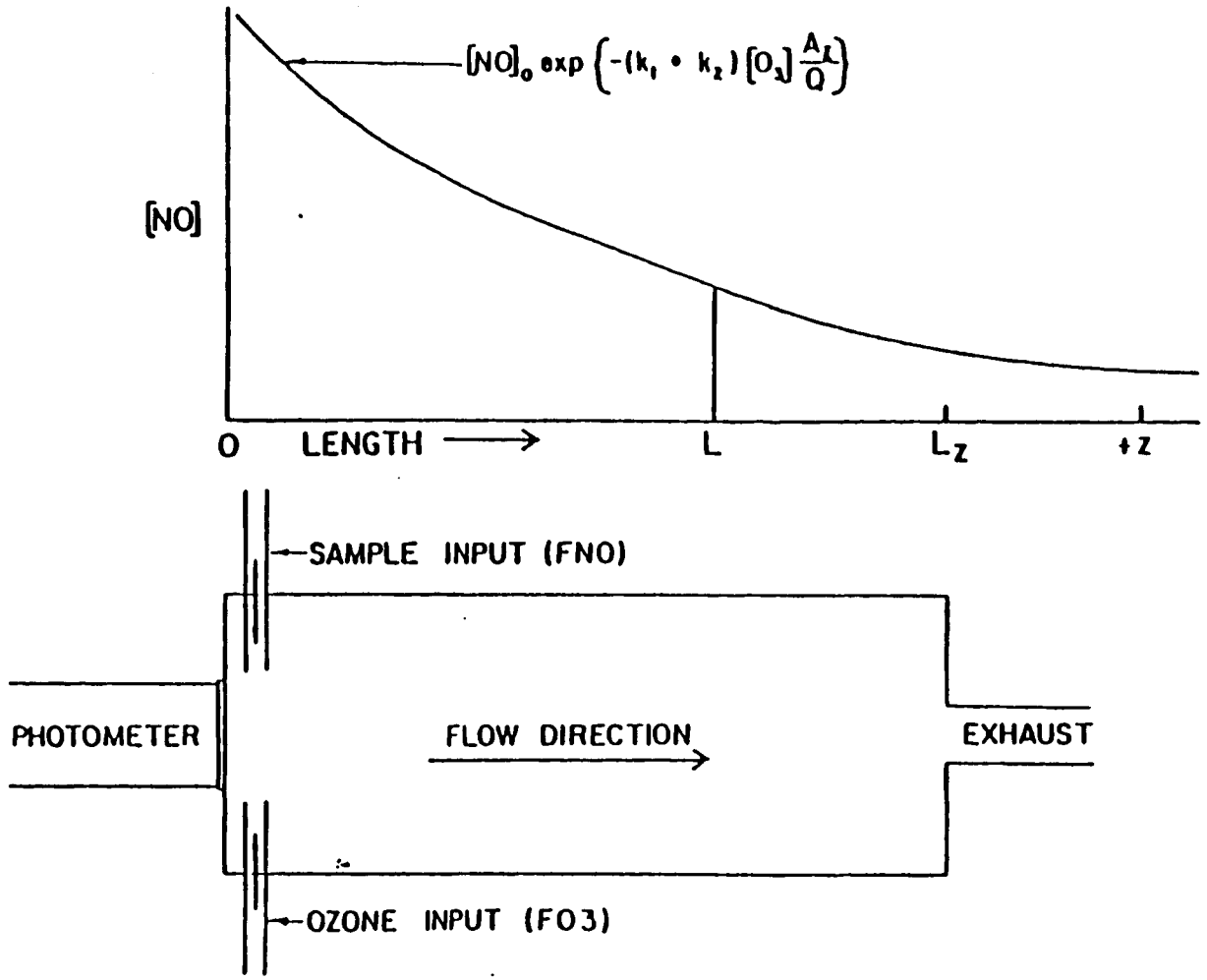

Figure (3) Block diagram of a cylindrical chamber which is represented as a plug flow reactor with reactant gas entering continuously at one end.

III. INSTRUMENT SENSITIVITY CALIBRATION

The parachute borne instrument is shown, to scale, in figure (1). Ambient air, $F_{(air)}$, is observed to enter at the inlet tube entrance, flow through the 70cm. long stainless steel inlet tube and into the 4.9cm. diameter reaction volume where it mixes with the reagent gas, $F_{(O_3)}$. The two gases enter , radially, through a series of equally spaced holes that lie in a plane parallel to, and directly in front of, the photomultiplier tube cathode. They continue through the reaction volume and are subsequently adsorbed on molecular sieves within a liquid nitrogen (LN2) cryo pump. Whenever ozone is introduced into a reaction volume two independent light emissions will be observed.

First, in the absence of nitric oxide an enhanced phototube signal is observed. Its magnitude, I_O, is strongly related to the prior time history of the ozone environment in the reaction chamber and for any given reaction chamber the quiesent value for 'I_O' is directly related to the ozone concentration. Its origin is thought to be directly related to a reaction of ozone with the surfaces of the reaction volume.

Second is a signal, $\mathbf{I_S}$, that is exactly proportional to the nitric oxide mixing ratio, $\Omega_{(NO)}$, in the ambient air flow as depicted by equation (13) and which results from the chemiluminescent reaction between nitric oxide and ozone. The proportionality factor, $\mathbf{YG(L)}$, is a variable which can be evaluated in terms of the variable instrument parameters, i.e., in terms of $F_{(air)}$, $\Omega_{(NO)}$, $F_{(O_3)}$, P_C, T, $\Omega_(O_3)$, *and* $\mathbf{I_S}$.

If, for purposes of calibration, equation (13) is rearranged to give

$$\mathbf{YG(L)} = \frac{\mathbf{I_S}(k_1 + k_2)kT_o\{1 + k_4P_C/k_3kT\}}{k_1P_oF_{(air)}\Omega_{(NO)}} \tag{14}$$

it is possible, using equations (11) and (14), to generate sets of data which cover the complete spectrum of flight related parameter values such that curves can be plotted. Analytical solutions can be obtained from these data which yield regression equations for $\mathbf{YG(L)}$ on L. Table I illustrates some partial data used to derive the calibration for instrument No D-4. The regression equation used to represent $\mathbf{YG(L)}$ for any given instrument takes the form

$$\mathbf{log(YG[L])} = a + b * log[L] = c * (log[L])^2 \tag{15}$$

where a,b,and c are arbitrary constants. Again for the D-4 instrument figure (4) shows, graphically, how the probability factor responds to reaction length. The solid curve represents a plot of the analytical expressions. The data used in their derivation was obtained in February 1980. The nitric oxide reference source, i.e., the standard, was a 53 PPMV (NO/N2) Matheson cylinder. Its contents were verified by comparison with a dilution of 100% feedback flow calibration system [Stedman et al.,1978]. Subsequent calibrations were obtained on 8/25/81 and 10/5/81 respectively. Both checks agree, within the statistical uncertainty, with the original model.

The probability factor, $\mathbf{YG(L)}$, is a dimensionless quantity which represents the ratio between observed photons and the total possible production of photons.

Rewriting equation (13), the instrument sensitivity can be expressed as

$$C_{(NO)} = \frac{k_1 P_o F_{(air)} \mathbf{YG(L)}}{(k_1 + k_2)\{1 + (k_4 P_C)/(k_3 kT)\}} \tag{16}$$

where $\Omega_{(NO)}$ has been set equal to 1 PPBV and $C_{(NO)}$ is defined as the nitric oxide mixing ratio sensitivity in counts/PPBV-sec. To this point there has been an apriori assumption about the instrument parameters, e.g., during the evaluation of $\mathbf{YG(L)}$ parameters were permitted to vary within limits yet to be defined. The following paragraphs will discuss the experimental flight environment and the resulting impact on the the variable flight parameters.

Table I

$F_{(air)}$	$F_{(O_3)}$	P_C	$\Omega_{(O_3)}$	T	$\Omega_{(NO)}$	I_S	L	$YG(L)$
0.666	0.569	0.459	0.0143	295.4	1.076E-6	74.707	68.42	3.314E-6
		0.787		295.5		105,156	23.24	7.929E-6
		1.386		295.5		118,881	7.47	1.572E-5
		2.171		295.5		106,557	3.05	2.202E-5
0.666	0.569	3.386	0.0143	295.6	1.076E-6	83,700	1.26	2.694E-5
0.457	0.589	0.413	0.0367	296.8	1.080E-6	137,965	22.36	7.865E-6
		0.828				148,592	5.56	1.682E-5
		1.382				121,172	2.00	2.280E-5
0.457	0.589	1.702	0.0367	296.8	1.080E-6	106,286	1.32	2.460E-5
0.682	0.589	0.474	0.0367	296.1	1.080E-6	168,830	25.29	7.483E-6
		0.799		296.1		195,257	8.90	1.432E-5
		1.219		296.2		179,041	3.82	2.008E-5
		1.615		296.3		153,188	2.17	2.344E-5
0.682	0.589	2.186	0.0367	296.3	1.080E-6	131,953	1.19	2.643E-5
10.170	0.589	2.222	0.0370	296.9	1.080E-6	218,146	81.57	2.955E-6
		2.604				246,100	59.39	3.905E-6
		3.138				279,844	40.90	5.348E-6
		3.886				314,896	26.47	7.448E-6
		4.904				337,687	16.62	1.008E-5
		5.972				353,684	11.21	1.285E-5
		6.947				359,441	8.28	1.519E-5
10.170	0.589	8.017	0.0370	296.9	1.080E-6	358,891	6.22	1.749E-5
0.668	0.571	0.466	0.0256	295.6	1.076E-6	122,781	37.07	5.495E-6
		0.799		295.7		154,986	12.59	1.180E-5
		1.269		295.7		154,270	4.99	1.858E-5
0.668	0.571	2.001	0.0256	295.7	1.076E-6	128,361	2.01	2.432E-5
0.642	0.255	0.347	0.0471	294.9	1.000E-7	14,649	42.76	5.515E-6
		3.047		294.9		9,988	0.56	3.234E-5
		1.316		294.9		16,013	2.95	2.247E-5
0.642	0.255	0.528	0.0471	294.8	1.000E-7	17.214	18.07	9.795E-6
0.641	0.255	2.881	0.0477	289.5	1.000E-7	9,571	0.66	3.157E-5
		1.289		289.7		14,684	3.30	2.175E-5
		0.976		289.7		15,965	5.76	1.794E-5
		0.752		289.7		16,148	9.70	1.401E-5
		0.534		289.9		15,059	19.24	9.314E-6
0.641	0.255	0.351	0.0477	289.9	1.000E-7	11,915	44.53	4.082E-6

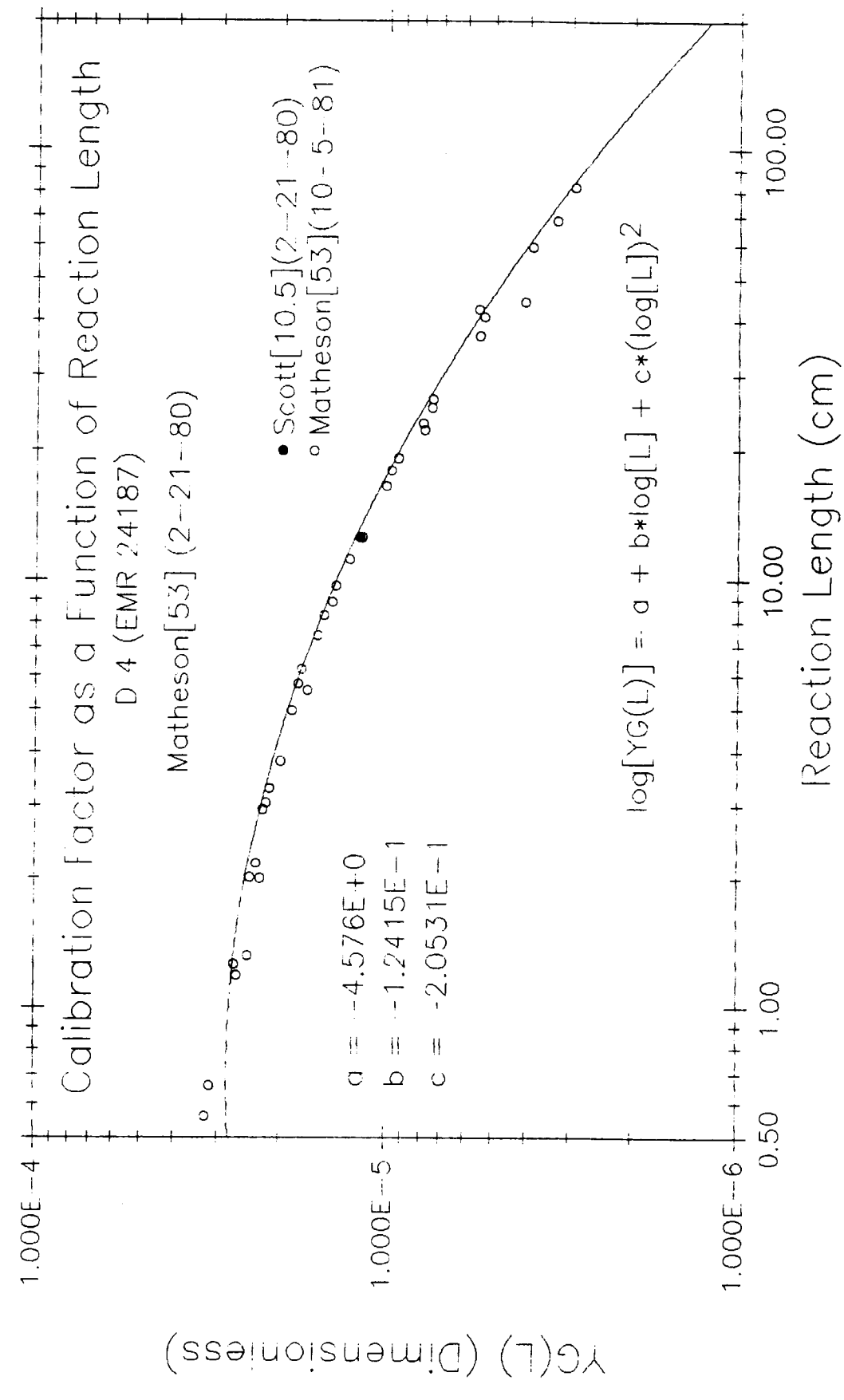

IV. INLET FLOW TUBE CALIBRATION

The mass flow rate of air, $F_{(air)}$, into the reaction chamber during a given flight experiment is determined by the conductance of the inlet flow tube. For viscous flow conditions the mass flow rate can be expressed, simply, in terms of the difference between the squares of the two pressures, i.e., $F_{air} = f[(P_t{}^2 - P_C{}^2]$, e.g., [Dushman], where P_t and P_C represent the enhanced ambient pressure and reaction chamber pressure respectively.

Figure (5) shows, graphically, two measured pressure profiles for NASA Flt. 30.008(typical). The lower dashed curve represents the output from a mechanical pressure transducer[Validyne] which continuously monitors the reaction volume pressure, P_C. The solid curve represents the ambient pressure data, P_a, obtained from a separate rocket payload, a Datasonde (Datasondes are specifically designed to yield relatively low cost measurements of atmospheric structure, i.e., the measurement of atmospheric temperature and horizontal winds) which, assuming hydrostatic equilibrium, results in solutions of ambient pressure and density. The actual pressure seen at the flow tube entrance is shown by the top dashed curve labeled P_t. This pressure profile is an enhanced ambient pressure curve caused by the instrument descent velocity, V, shown in figure(6). The top two pressure curves are related, analytically, by the isentropic relation

$$\frac{P_t}{P_a} = \left(1 + \frac{\gamma - 1}{2} M^2\right)^{\frac{\gamma}{\gamma - 1}}$$

where the Mach number, $M = V/c$, is less then unity, c is the local speed of sound, and the ratio of specific heats $\gamma = 1.4$ (air).

Having established the range of pressures that can be expected to exist (figure 5) the inlet flow tube can be calibrated in the laboratory. The calibration is simply a matter of generating a set of observations of mass flow rate in terms of known pressures, Table II, such that linear, second order, regression curves can be derived (by least squares) for $F_{(air)}$ on ΔP^2 where

$$\Delta P^2 = P_t{}^2 - P_C{}^2.$$

Notice that the base data has been plotted on three separate graphs (figures 7,8, and 9) according to the different ranges of ΔP^2 and that three regression equations have been derived with corresponding correlation coefficients, r^2. Segmenting the data in this manner improves the precision within each data group.

For a given set of flight pressure information, e.g., figure 5, the regression equations for $F_{(air)}$ on ΔP^2 can be used to derive the ambient sample flow rate at any given altitude (time). Figure 10 illustrates the derived flow rate on altitude for Flt. 30.008 and instrument D-4. The error bars shown are based upon the, assumed, uncertainty in P_t,i.e., $\pm 5\%$ above 35 km. and $\pm 2.5\%$ be-low 35 km.

Notice that the maximum observed flow rate in figure (10 is just over 10cc/sec., reached on descent, at an altitude of about 33km. As the instrument continues its descent the ambient flow rate actually decreases untill at 30 km. it has a value on the order of 2.5 cc/sec. Recall the the flow of gases is maintained through this instrument by a cryogenic pump. The decreasing flow rate at the lowest altitudes is a symptom that the refrigerated adsorbent in the pump has been heated by previously adsorbed gases to a point where it can no longer pump ideally.

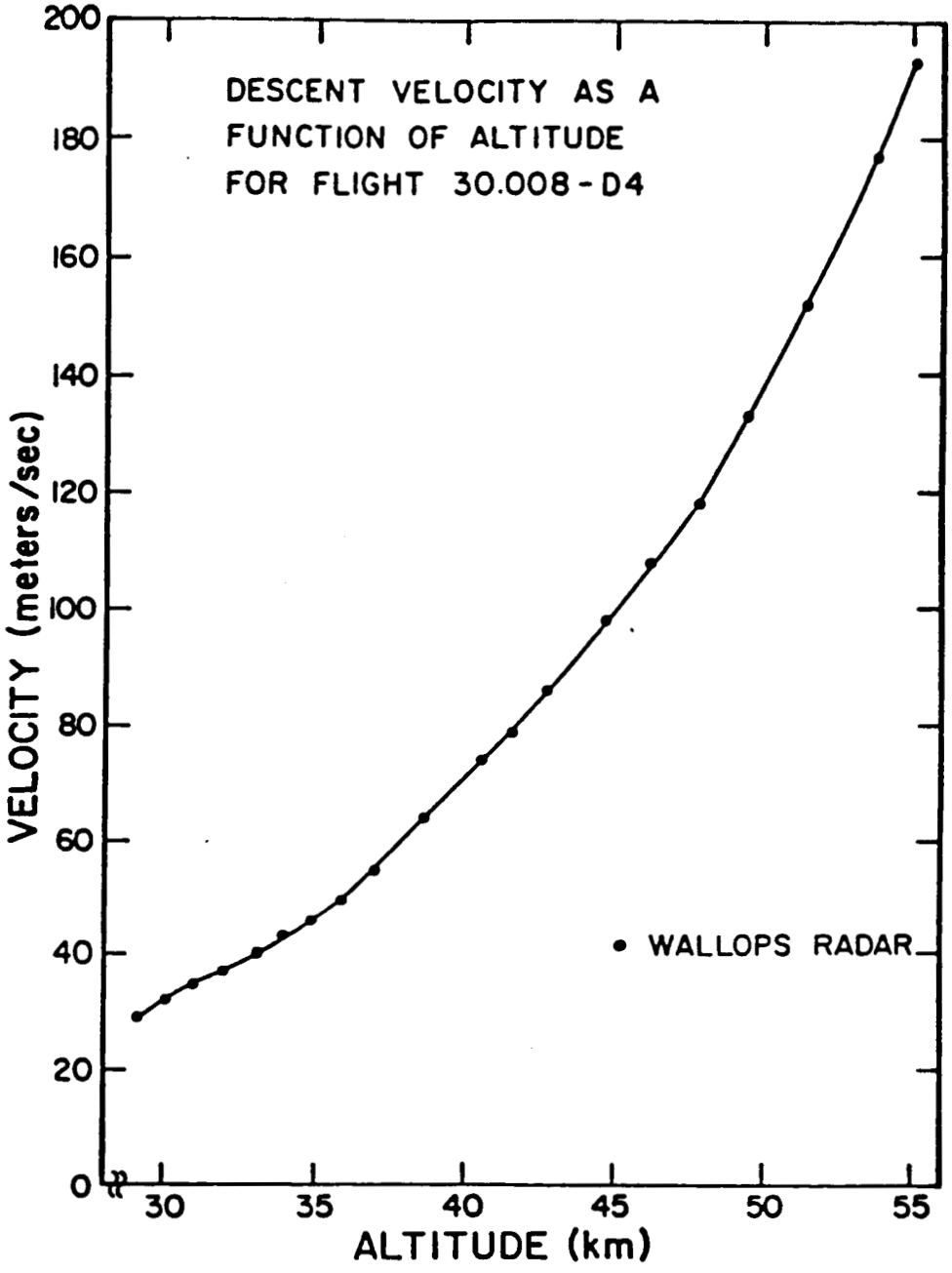
DESCENT VELOCITY AS A
FUNCTION OF ALTITUDE
FOR FLIGHT 30.008-D4
VELOCITY (meters/sec)
ALTITUDE (km)
• WALLOPS RADAR
0
20
40
60
80
100
120
140
160
180
200
30
35
40
45
50
55

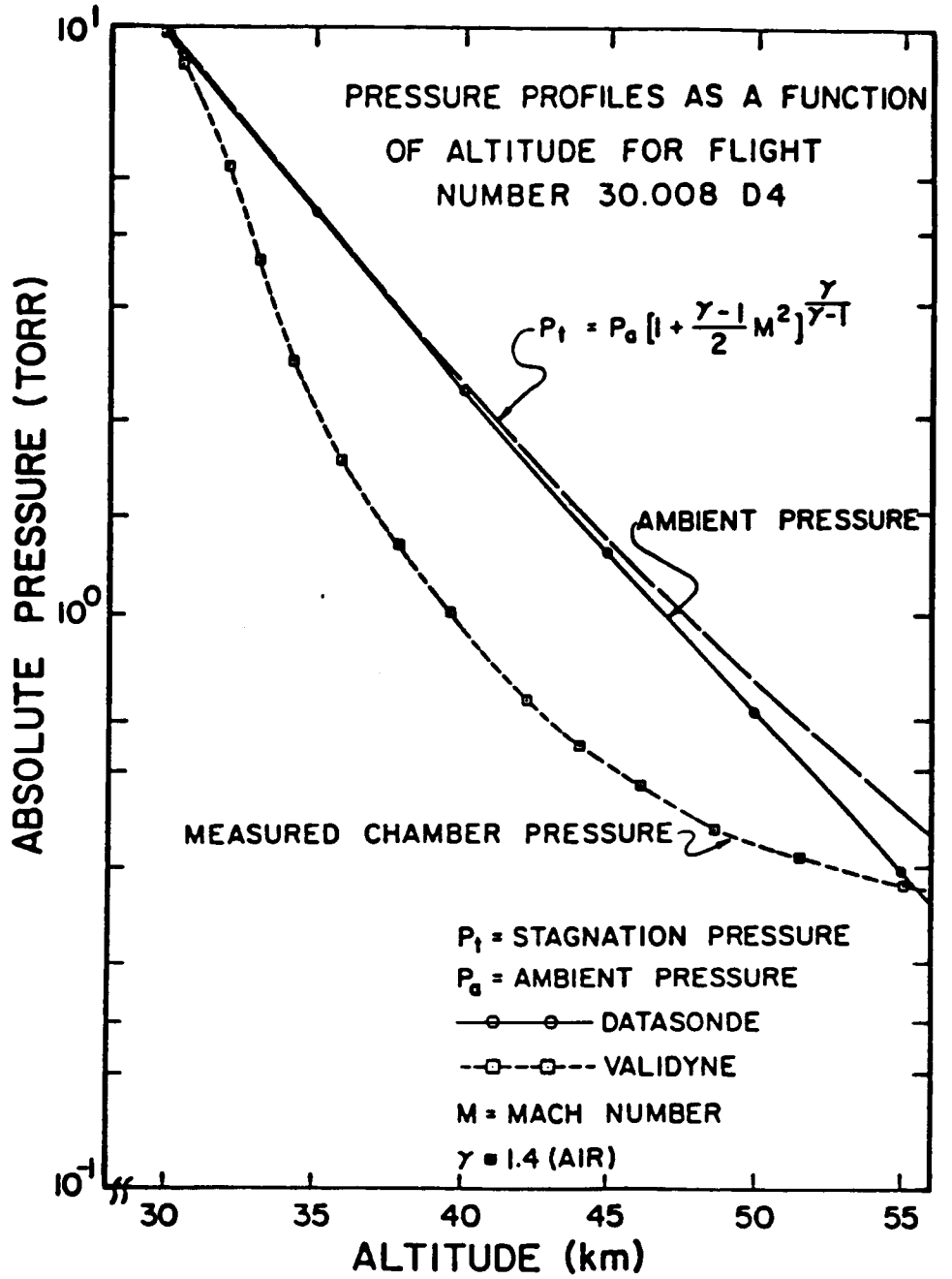
PRESSURE PROFILES AS A FUNCTION OF ALTITUDE FOR FLIGHT NUMBER 30.008 D4
$P_t = P_a\left[1 + \frac{\gamma-1}{2}M^2\right]^{\frac{\gamma}{\gamma-1}}$
AMBIENT PRESSURE
MEASURED CHAMBER PRESSURE
P_t = STAGNATION PRESSURE
P_a = AMBIENT PRESSURE
DATASONDE
VALIDYNE
M = MACH NUMBER
γ = 1.4 (AIR)
ABSOLUTE PRESSURE (TORR)
10^1
10^0
10^{-1}
30
35
40
45
50
55
ALTITUDE (km)

TABLE II

P_t	P_C	ΔP^2	$F_{(air)}$
0.555	0.329	0.200	0.123
0.667	0.351	0.322	0.197
0.812	0.379	0.516	0.307
0.900	0.398	0.652	0.382
1.013	0.426	0.845	0.492
1.126	0.457	1.059	0.606
1.261	0.494	1.346	0.761
1.383	0.533	1.629	0.914
1.577	0.597	2.131	1.204
1.777	0.666	2.714	1.530
1.956	0.731	3.292	1.832
2.313	0.878	4.579	2.524
2.722	1.062	6.281	3.409
2.971	1.178	7.439	3.978
3.377	1.362	9.549	5.044
2.311	0.871	4.582	2.510
2.720	1.055	6.285	3.409
2.973	1.174	7.460	4.007
3.377	1.362	9.549	5.044
3.781	1.559	11.865	6.142
4.203	1.773	14.522	7.342
4.597	1.980	17.212	8.534
5.061	2.231	20.636	9.975
5.428	2.435	23.534	11.151
5.883	2.696	27.341	12.779
6.900	3.299	36.727	16.648
7.988	3.973	48.023	20.557
9.870	8.777	20.527	9.933

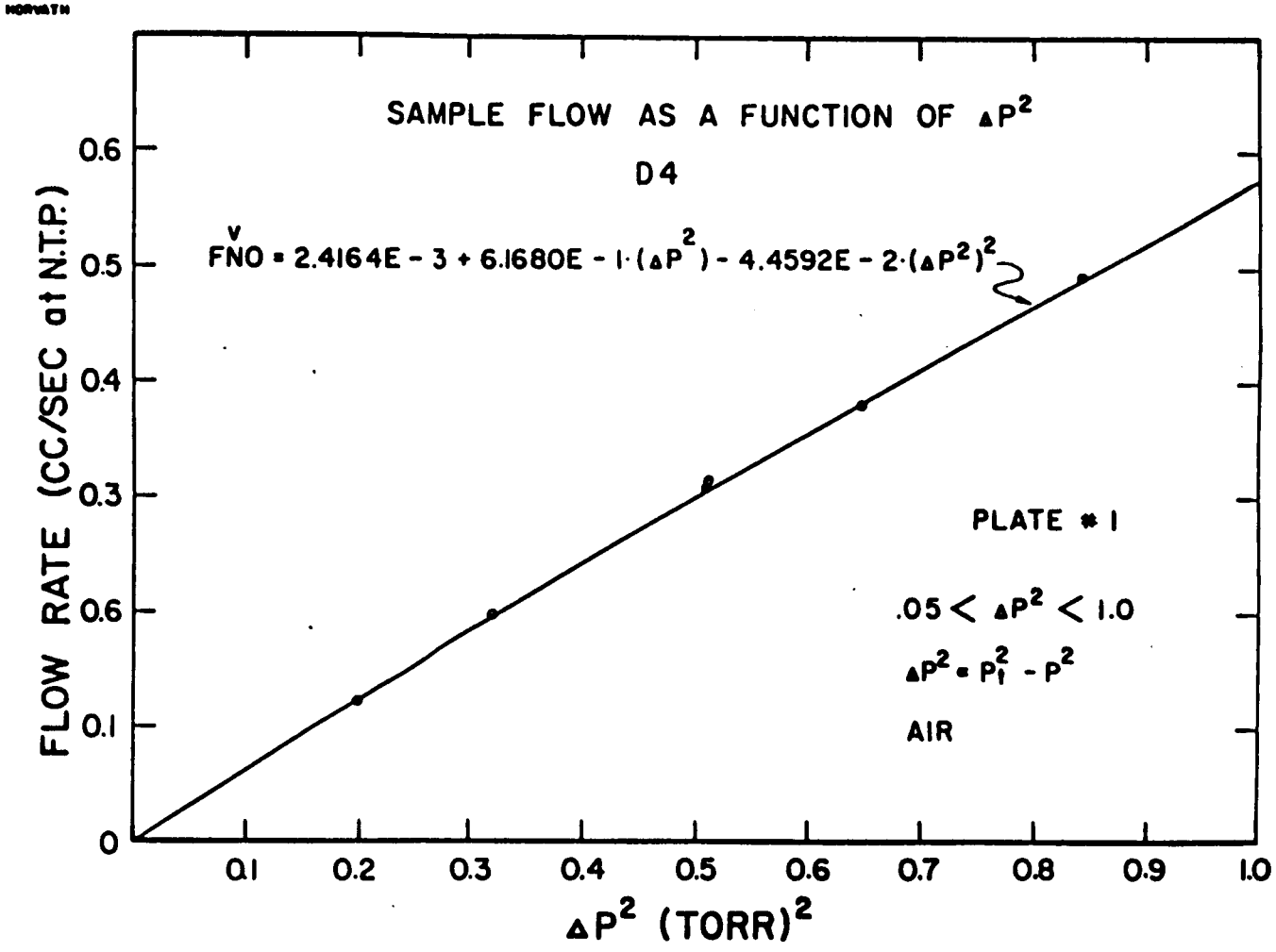
SAMPLE FLOW AS A FUNCTION OF ΔP²
D4
V
FNO = 2.4164E - 3 + 6.1680E - 1·(ΔP²) - 4.4592E - 2·(ΔP²)²
PLATE # 1
.05 < ΔP² < 1.0
ΔP² = P₁² - P²
AIR
FLOW RATE (CC/SEC at N.T.P.)
0
0.1
0.6
0.3
0.4
0.5
0.6
0.1
0.2
0.3
0.4
0.5
0.6
0.7
0.8
0.9
1.0
ΔP² (TORR)²

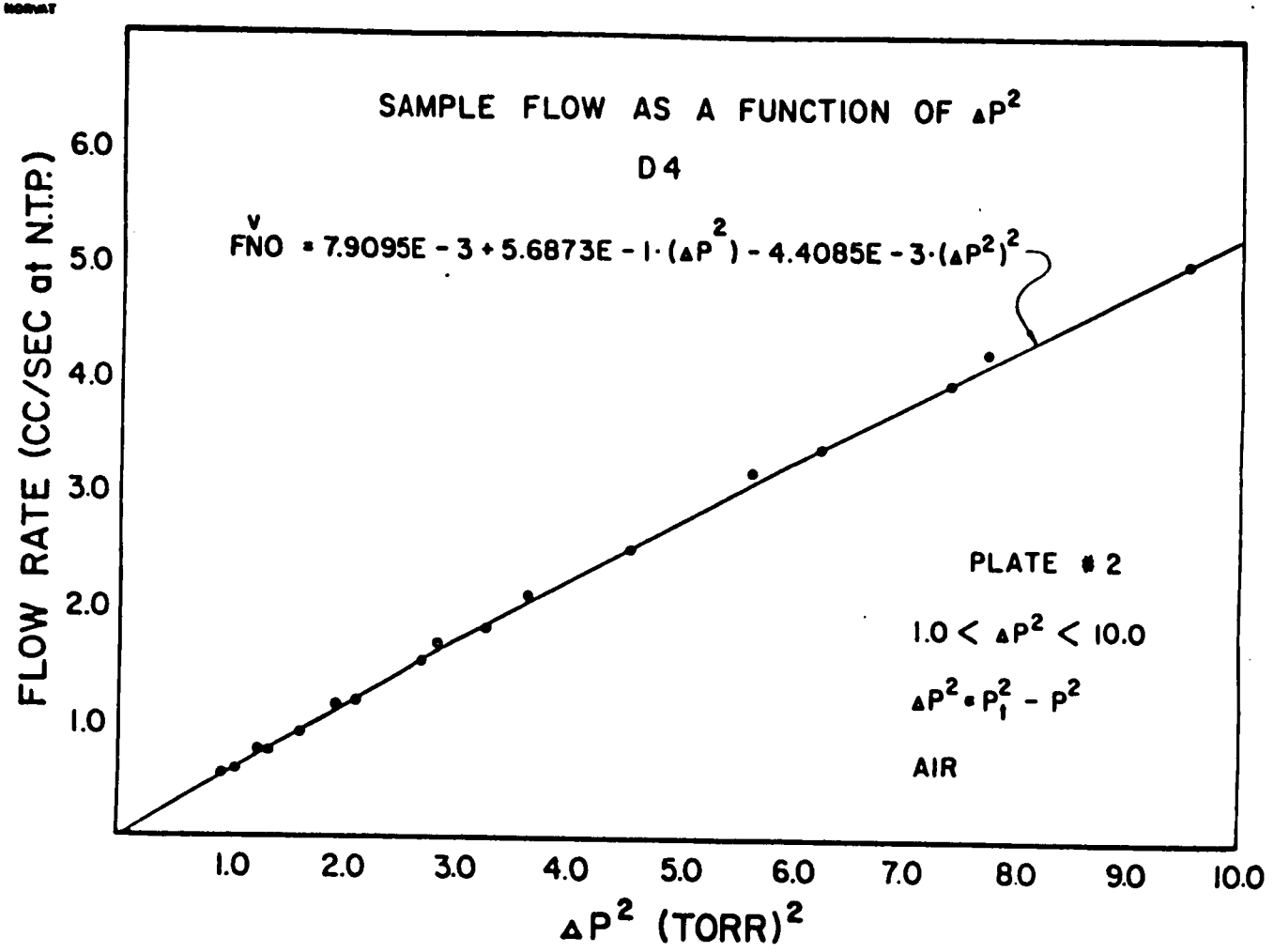
SAMPLE FLOW AS A FUNCTION OF ΔP²
D 4
V
FNO = 7.9095E - 3 + 5.6873E - 1·(ΔP²) - 4.4085E - 3·(ΔP²)²
PLATE # 2
1.0 < ΔP² < 10.0
ΔP² = P₁² - P²
AIR
FLOW RATE (CC/SEC at N.T.P.)
1.0
2.0
3.0
4.0
5.0
6.0
1.0
2.0
3.0
4.0
5.0
6.0
7.0
8.0
9.0
10.0
ΔP² (TORR)²

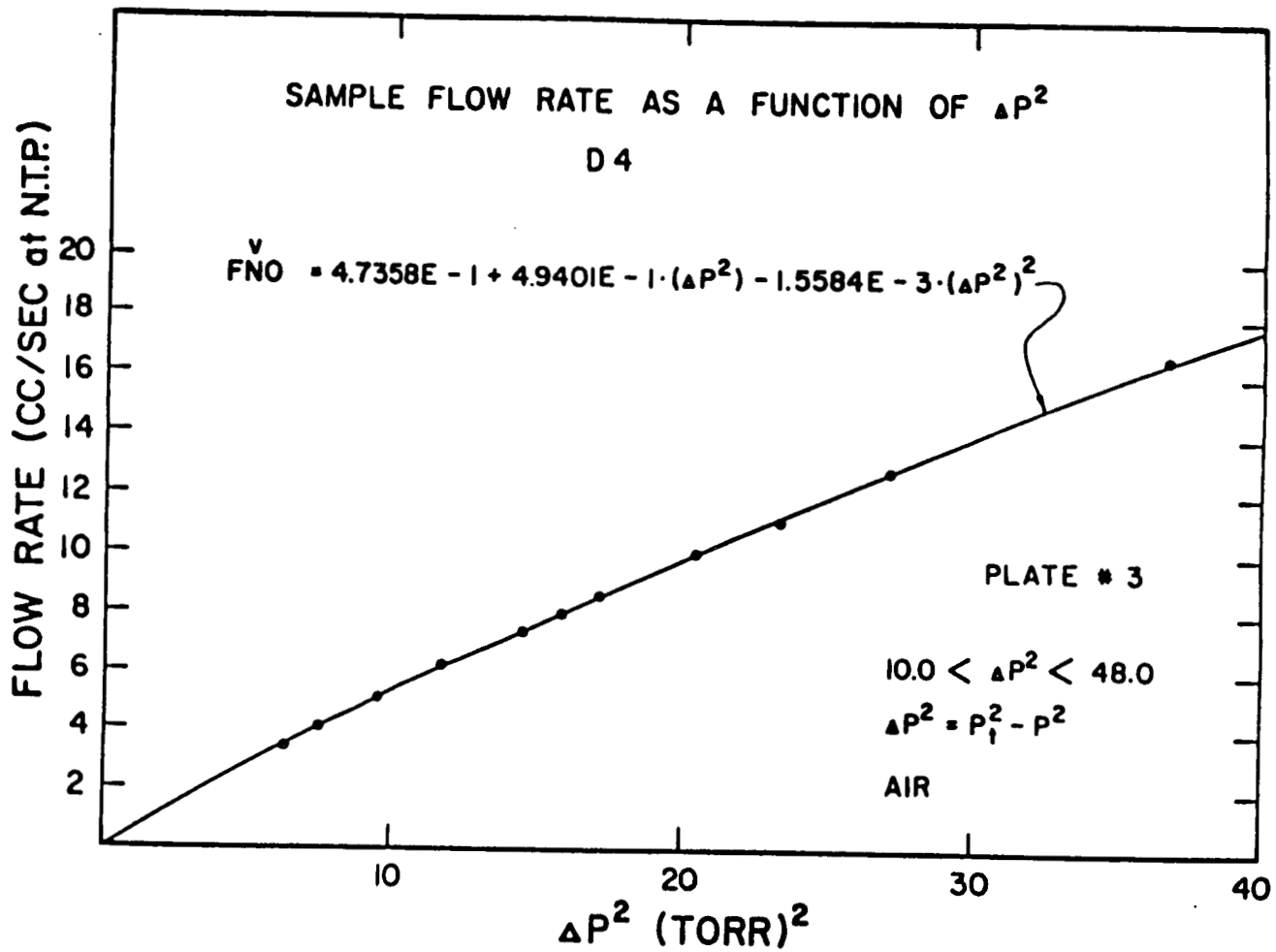
SAMPLE FLOW RATE AS A FUNCTION OF ΔP²
D 4
V
FNO = 4.7358E - 1 + 4.9401E - 1·(ΔP²) - 1.5584E - 3·(ΔP²)²
PLATE # 3
10.0 < ΔP² < 48.0
ΔP² = P₁² - P²
AIR
FLOW RATE (CC/SEC at N.T.P.)
2
4
6
8
10
12
14
16
18
20
10
20
30
40
ΔP² (TORR)²

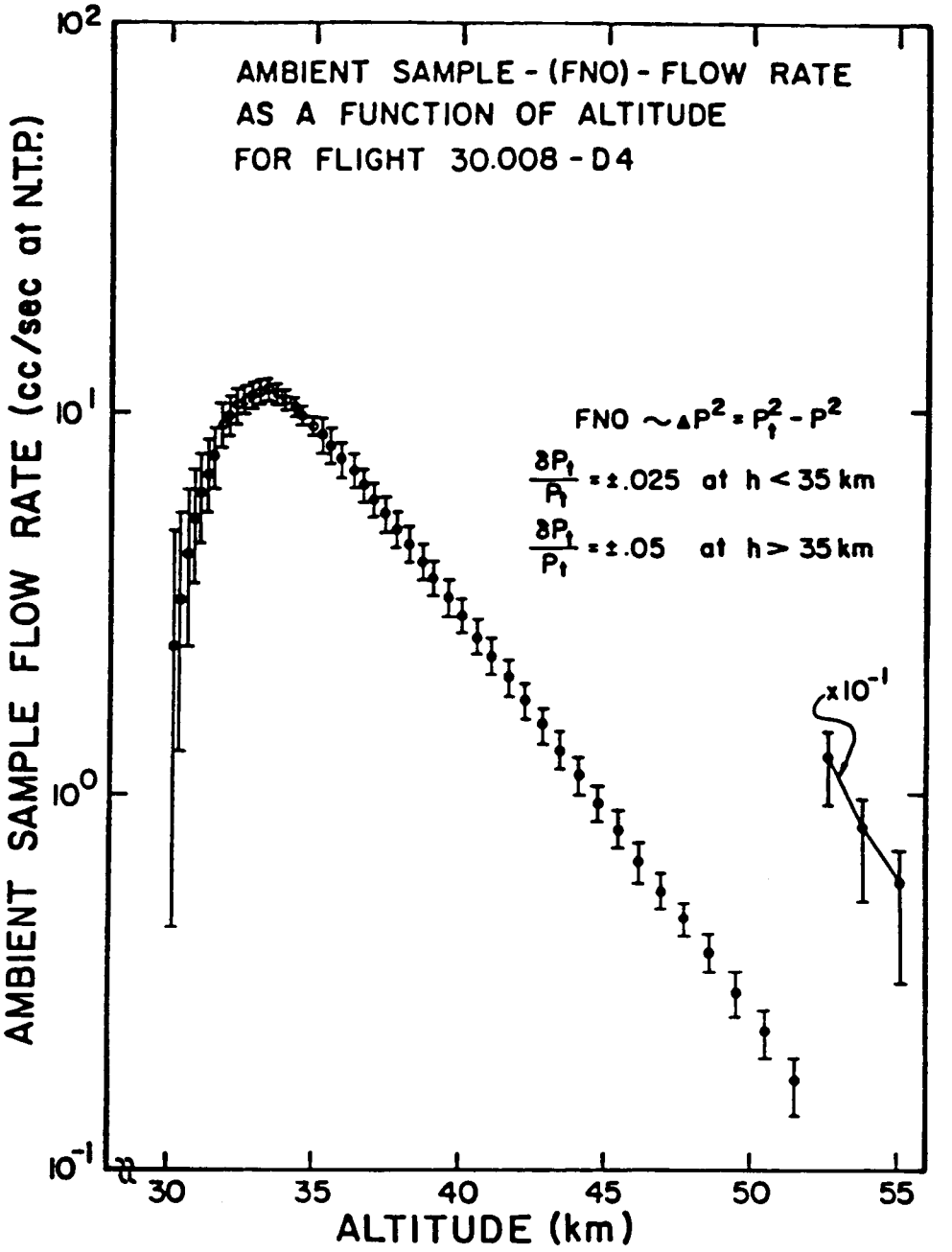
AMBIENT SAMPLE - (FNO) - FLOW RATE
AS A FUNCTION OF ALTITUDE
FOR FLIGHT 30.008 - D4
FNO ~ΔP² = P₁² - P²
δP₁/P₁ = ±.025 at h < 35 km
δP₁/P₁ = ±.05 at h > 35 km
x10⁻¹
AMBIENT SAMPLE FLOW RATE (cc/sec at N.T.P.)
ALTITUDE (km)
10²
10¹
10⁰
10⁻¹
30
35
40
45
50
55

V. OZONE/OXYGEN CONCENTRATION - $\Omega(O_3)$

The ozone systems related to the parachute borne instrument consist of: (1) the laboratory production of ozone, (2) the storage of ozone aboard the instrument and (3) the distribution of ozone during the measurement of nitric oxide.

Ozone is produced in the laboratory by passing oxygen through a laboratory ozone generator. With the oxygen flow rate adjusted to 1.0 cc/sec. (@ NTP) ozone is produced at a constant value on the order of 5.5 mole-percent.

This ozone/oxygen mixture can be directed into, and through, the stainless steel instrument storage vessel via two manually operated access valves. Continuous flow of this ozone enriched gas over extended periods of time tends to passivate the container surfaces such that ozone can be stored at some initial concentration, $\Omega(O_3)_1$, and then be retrieved for experimental purposes at some later time with a known(predicted) concentration $\Omega(O_3)_2$. This ratio,

$$\frac{\Omega(O_3)_1}{\Omega(O_3)_2} = R$$

can be evaluated statistically on the basis of repeated laboratory experiments prior to a rocket experiment. An example of this procedure is illustrated in Table III. The object is to derive the most recent time history of $\Omega(O_3)$ as a function of time between events 1 and 2. The seven test results that are illustrated here preceded the 23 July 1981 launch of intrument D-4. The ozone concentration measurements were carried out by UV absorbtion at 254nm. using an absorbtion cell having a path length of 0.100 cm.

Inspection of Table III shows that ozone can be expected to reside in the storage volume with very little loss over extended periods of time as evidenced by the fact that the mean value of R for the seven test results is 0.990 over the time period on the order of 20 hours. The typical required storage time, relative to a rocket launched experiment, is 2-3 hours.

TABLE III

OZONE CONCENTRATION RESIDENCE TIME
Prelaunch Data for Flight 30.008

$Date_1$	$Time_1$	$\Omega_{(O_3)_1}$	$Date_2$	$Time_2$	$\Omega_{(O_3)_2}$	t	R
7-14-81	14:30	0.05280	7-15-81	09:00	0.05294	18:30	1.0027
7-15-81	11:00	0.05708	7-16-81	008:30	0.05640	21:30	0.9893
7-16-81	09:55	0.05478	7-17-81	08:45	0.05502	22:50	1.0044
7-17-81	14:55	0.05484	7-18-81	08:35	0.05445	17:40	0.9929
7-20-81	10:04	0.05649	7-21-81	08:04	0.05486	22:00	0.9711
7-21-81	09:38	0.05395	7-22-81	08:01	0.05358	22:23	0.9931
7-22-81	09:35	0.05527	7-23-81	07:46	0.05324	22:11	0.9792

$Date_1$ and $Time_1$ = ozone valve close time conditions.

$Date_2$ and $Time_2$ = ozone valve open time conditions.

t=ozone storage time in hours

Residence time ratio

$$R = \frac{\Omega_{(O_3)_2}}{\Omega_{(O_3)_1}}$$

VI. OZONE/OXYGEN FLOW RATE-F_{O_3}

The reagent gas is carried aboard the chemiluminescent instrument in a 692cc., vacuum brazed stainless steel, storage volume. This volume exists in the annular region concentric about the instrument reaction volume. The gas is stored, for experimental usage, at existing the laboratory barometric pressure and can be admitted into the reaction chamber for calibration and/or experimental purposes by opening a specially designed, pyrotechnic actuated, bellows valve assembly whereupon the gas flow rate, F_{O_3}, is governed by porous stainless steel flow restrictor[MOTT]. The flow restrictor is statically calibrated over the full range of expected storage volume pressures and a linear least squares curve fit is generated (Figure 11).

For static conditions where the ozone volume is continuously vented to the laboratory environment, e.g., during instrument calibrations where laboratory produced ozone continuously purges the storage resevoir, the reagent gas flow (F_{O_3}) can be predicted from a measure of the barometric pressure and application of the static calibration equation.

For the dynamic situation which is encountered during a rocket borne flight it becomes necessary to determine the rate of pressure change in the storage vessel as the reagent gas is being consumed. This can be accomplished by iterating the expression

$$V dP_{O_3} = F P_{O_3} dt \tag{17}$$

with

$$F_p = \frac{F_{O_3} 760}{P_{O_3}}$$

where V is the ozone storage volume in cc., P_{O_3} is the pressure in the storage volume, dp_{O_3} is the rate of change in P_{O_3}, and F_P is the volume flow rate of the reagent gas at pressure P_{O_3}. Figure (12) illustrates a flight time history for a comparison between the predicted ozone storage volume pressure based upon the application of equation (17) and the actual pressure measurement[Kulite].

A typical reagent gas flow rate curve, F_{O_3} on altitude, is presented in figure (13) along with an assigned uncertainty in the measurement of $\pm 2.5\%$.

Figure 11

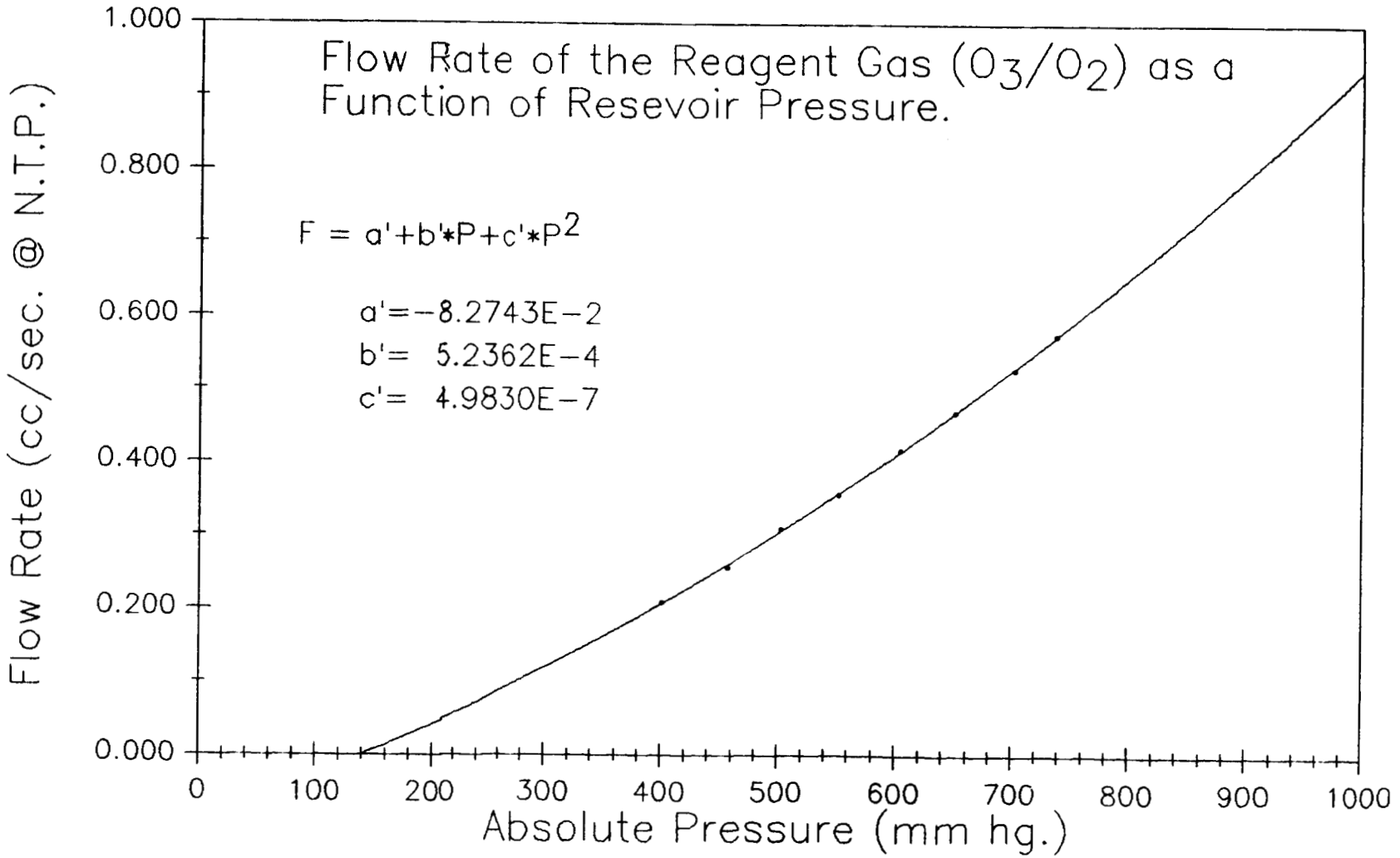
Flow Rate of the Reagent Gas (O_3/O_2) as a Function of Resevoir Pressure.
$F = a' + b'*P + c'*P^2$
a'=−8.2743E−2
b'= 5.2362E−4
c'= 4.9830E−7
Flow Rate (cc/sec. @ N.T.P.)
1.000
0.800
0.600
0.400
0.200
0.000
0
100
200
300
400
500
600
700
800
900
1000
Absolute Pressure (mm hg.)

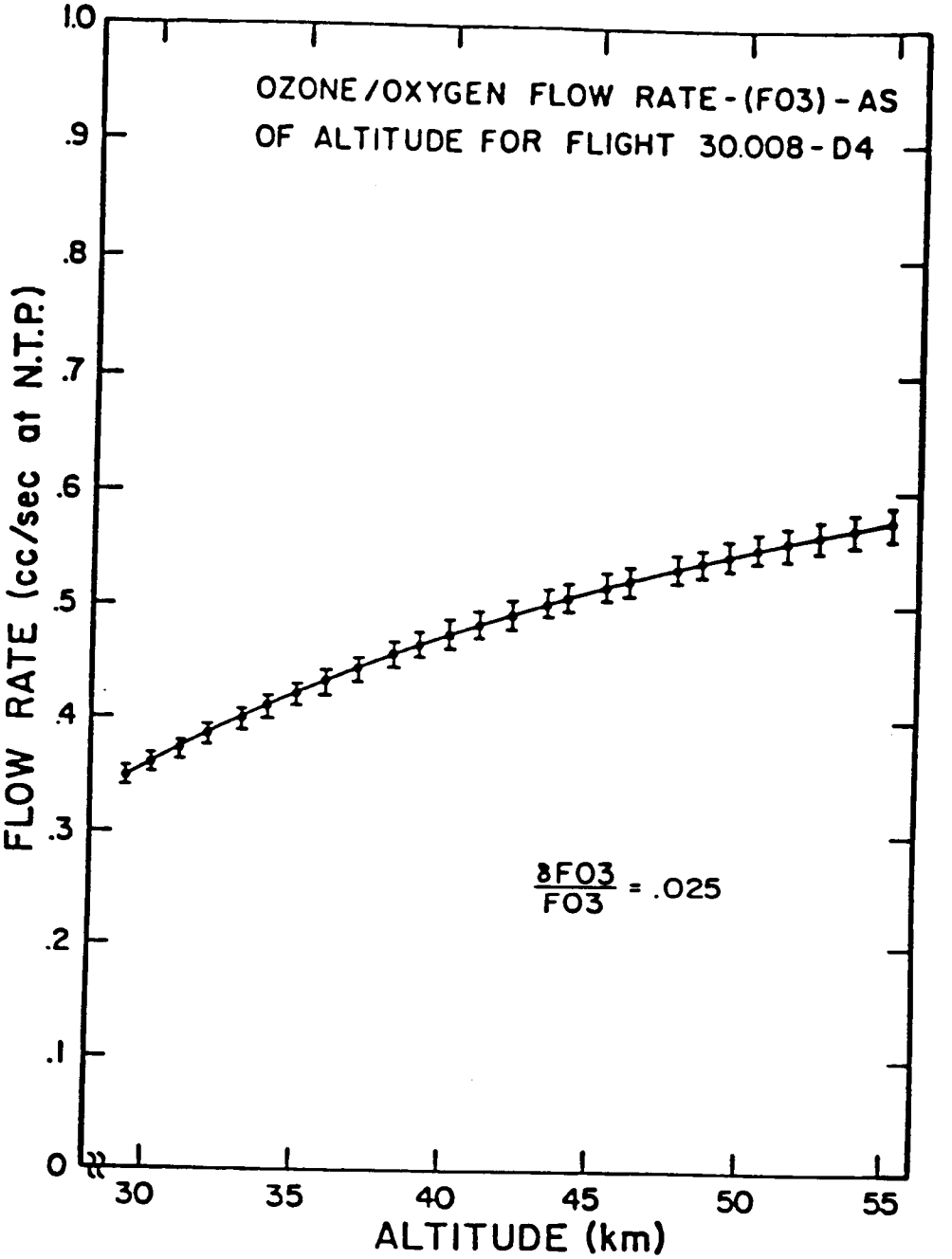
OZONE/OXYGEN FLOW RATE - (FO3) - AS
OF ALTITUDE FOR FLIGHT 30.008 - D4
FLOW RATE (cc/sec at N.T.P.)
1.0
.9
.8
.7
.6
.5
.4
.3
.2
.1
0
30
35
40
45
50
55
ALTITUDE (km)
δFO3/FO3 = .025

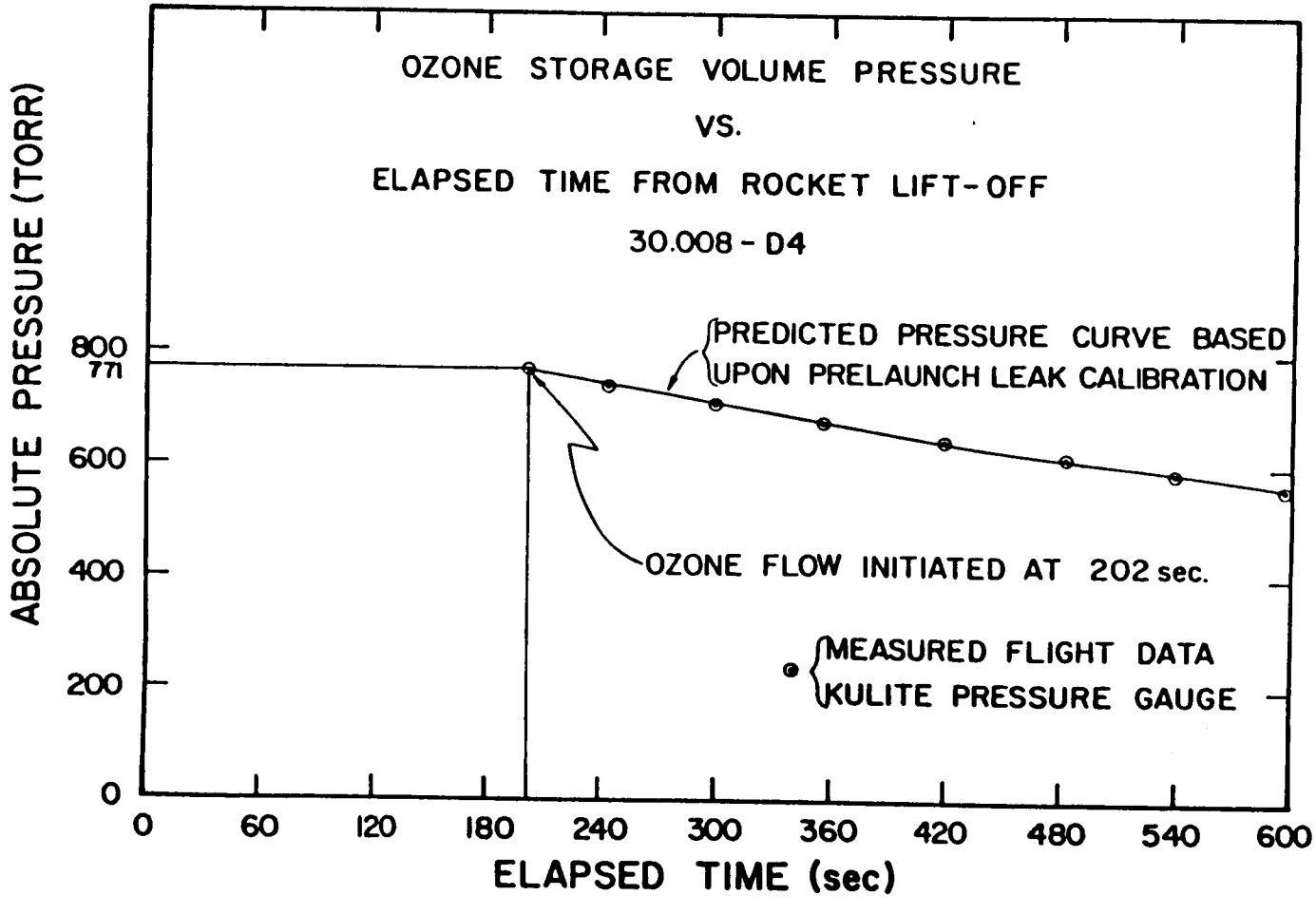
OZONE STORAGE VOLUME PRESSURE
VS.
ELAPSED TIME FROM ROCKET LIFT-OFF
30.008 - D4
PREDICTED PRESSURE CURVE BASED
UPON PRELAUNCH LEAK CALIBRATION
OZONE FLOW INITIATED AT 202 sec.
MEASURED FLIGHT DATA
KULITE PRESSURE GAUGE
ABSOLUTE PRESSURE (TORR)
800
600
400
200
0
0
60
120
180
240
300
360
420
480
540
600
ELAPSED TIME (sec)

VII. REACTION CHAMBER PRESSURE-P_C

The reaction chamber pressure, P_C, is measured continuously during an experiment by an absolute mechanical pressure transducer[Validyne]. An example of the derived pressure profile from such a gauge was given, previously, in figure (5). Calibration of the pressure transducer is carried out before and after each flight.

Calibrations are performed using a descrete pressure-increment technique[Flanick and Ainsworth,1961] and with an M.K.S. Baratron reference standard. The methodology is as follows. Small descrete volumes, V_2, containing dry air at one atmosphere are incrementally added to a large resevoir, V_1, which is initially evacuated. Volumes V_2 and V_1 are approximately 30cc. and 55,000cc., respectively, and yield incremental pressure step sizes on the order of 0.4 Torr/step. Incrementing the calibration steps in this manner is a convienient way to ensure equal wieghting of data.

After the entire 10 Torr pressure scale has been covered, a linear least squares curve fit is employed to obtain an analytic solution for pressure as a function of transducer output signal.

An example of the preflight and postflight pressure calibration results for Flt. 30.008 are

$$P_C = -0.3979 + 2.11085 * E_V\ Torr \quad r^2 = 0.999972 \quad \text{[Pre-Flight]}$$
$$P_C = -0.4806 + 2.11151 * E_V\ Torr \quad r^2 = 0.999955 \quad \text{[Post-Flight]}$$

where E_V is the Validyne pressure transducer output voltage(Volts). The important parameter,i.e., the sensitivity, is shown to be vitually unchanged and is typical of this transducer operation.

The offset voltage(found by setting P_C equal to zero) has changed by 0.039 volts which is not uncommon in mechanical devices. This is, most likely, the result of the diaphram deformation which can be traced to the pressure environment immediately preceeding a gauge calibration. The AP 78 Validyne pressure transducer also has a slight orientation offset, due to the mass of the diaphram, on the order of 0.025 volts depending upon the up-down position of the gauge. The total offset voltage is evaluated for any given flight, continuously, from rocket lift-off until sometime after instrument separation during which time the cryogenic pump is maintaining a 'zero' pressure environment in the reaction volume.

VIII. GAS TEMPERATURE

The temperature environment of the instrument is monitored by seven precision thermisters which are located on the external surfaces on and about the reaction vessel. For gas temperature considerations thermal accommodation is assumed [Kays,1955] and that reaction that takes place in the reaction chamber is coincident with these measured values.

One decided advantage with regard to a rocket launched experiment is the relatively short time which the instrument is exposed to a hostile environment. The total period of time from rocket lift-off until the measurement is completed, at approximately $30km.$, is about 10 minutes. For example, the mean measured temperatures at the start and finish of the experiment for Flt. 30.008 were 297.2 ± 0.5 and 297.4 ± 0.2 respectively.

IX. PSL–PCM–TELEMETRY SYSTEM

The telemetry package, developed by the Physical Science Laboratory (PSL) of New Mexico State University, was designed to fit the small diameter payloads typically flown on rockets such as the Arcas. This package, measuring 5.0 inches long by 4.0 inches in diameter, contains a digitizer, a pulse code modulator, an L-band transmitter, an antenna, and a power supply. The package has been a standard for years for its small size, good performance, and low cost.

To satisfy the NASA design requirement for the package to be expendable and low cost, PSL used an RCA cavity oscillator (vacuum tube) for the transmitter. Not only is this transmitter somewhat unstable in frequency untill thoroughly warmed up, but if one intends to recover the payload, one must carefully evaluate the reuse of the package after each flight considering the fragility of the tube.

The PCM system is somewhat specialized, having a small frame size and no programmability except for the bit rate (a crystal replacement). The original PSL design provided for 8 channels of analog input, each channel being digitized into 8 bit words. One 8 bit sync word is used each frame, giving a total frame size of 9 words (72 bits). The standard PSL system was modified for the Michigan rocket payload to provide six analog inputs and one serial digital input channel. The encoder logic replaces what would have been the 7 th analog word with the 8 bits of information being received on the digital channel during that time in the frame and replaces the 8 th analog word with the next 8 bits received on the digital input. Michigan uses a bit rate of 7.2 khz to achieve a frame rate of 100 frames per second. The full scale input level to an analog channel is +5.10 volts. The pulse code modulation is 'bi-phase level'.

The power supply delivers high voltage to the RCA tube, low voltage to the PCM encoder logic and, in addition, supplies an unregulated ±15 volts to the experimenters instrument. The filament for the vacuum tube transmitter runs directly off the battery. For the Michigan payload, source power is derived from 5 PMC 2.5 silver cells, which can provide 7 volts at 1.5 ammperes for well over 30 minutes.

The stripline array antenna is a printed circuit which wraps around the fibreglass exterior of the package. It is tuned to radiate at 1680 mhz ±1%. The output power is approximately 1/4 watt.

X. ERROR ANALYSIS OF GAUGE PRESSURES

The basic calibration equation results from a second order least squares curve fit of pressure on gauge output voltage, i.e.,

$$P_{cal} = \alpha + \beta E + \gamma E^2 \tag{18}$$

where

$$E = E_e + ZPV_{cal}$$

with E, E_e, and ZPV_{cal} defined to be the gauge output voltage, the effective gauge output voltage, and the 'zero pressure' voltage respectively. Since the ZPV can be expected to vary over time for any number of reasons we need to take the ZPV change into account when using equation (18) to evaluate the pressure environment. For example, we can rewrite equation (18) to include ZPV values during calibration and flight respectively, i.e.,

$$P_{flt} = \alpha + \beta[E_e + ZPV_{cal} + \Delta ZPV] + \gamma[E_e + ZPV_{cal} + \Delta ZPV]^2 \tag{19}$$

where $\Delta ZPV = ZPV_{cal} - ZPV_{flt}$. Equation (19) can be expanded to give

$$P_{flt} = \alpha + \beta[E_e + ZPV_{cal} + ZPV_{cal} - ZPV_{flt}] + \gamma[E_e + ZPV_{cal} + ZPV_{cal} - ZPV_{flt}]^2$$

and finally

$$P_{flt} = \alpha + \beta[E + ZPV_{cal} - ZPV_{flt}] + \gamma[E + ZPV_{cal} - ZPV_{flt}]^2 \tag{20}$$

where ZPV_{cal} and ZPV_{flt} are the 'zero pressure' gauge offset voltages for conditions during calibration and flight respectively. From equation (20) the variables are seen to be

α, β, γ, E, ZPV_{cal}, and ZPV_{flt}.

along with the corresponding uncertainties

$\delta\alpha$, $\delta\beta$, $\delta\gamma$, δE, δZPV_{cal}, and δZPV_{flt}.

The uncertainty in the calculated pressure as a function of the uncertainty in the variables can be expressed as

$$\delta P = \left[\left(\frac{\partial P}{\partial \alpha}\right)^2 (\delta\alpha)^2 + \left(\frac{\partial P}{\partial \beta}\right)^2 (\delta\beta)^2 + \left(\frac{\partial P}{\partial \gamma}\right)^2 (\delta\gamma)^2 + \left(\frac{\partial P}{\partial E}\right)^2 (\delta E)^2 + \left(\frac{\partial P}{\partial ZPV_{cal}}\right)^2 (\delta ZPV_{cal})^2 + \left(\frac{\partial P}{\partial ZPV_{flt}}\right)^2 (\delta ZPV_{flt})^2\right]^{\frac{1}{2}} \tag{21}$$

The partial derivatives in terms of the variables are

$$\frac{\partial P}{\partial \alpha} = 1,$$
$$\frac{\partial P}{\partial \beta} = E + ZPV_{cal} - ZPV_{flt},$$
$$\frac{\partial P}{\partial \gamma} = (E + ZPV_{cal} - ZPV_{flt})^2,$$
$$\frac{\partial P}{\partial E} = \beta + 2\gamma(E + ZPV_{cal} - ZPV_{flt}),$$
$$\frac{\partial P}{\partial ZPV_{cal}} = \beta + 2\gamma(E + ZPV_{cal} - ZPV_{flt}),$$
$$\frac{\partial P}{\partial ZPV_{flt}} = -[\beta + 2\gamma(E + ZPV_{cal} - ZPV_{flt})].$$

Now equation (21) can be rewitten as

$$\delta P = \left[(\alpha)^2\left(\frac{\partial P}{\partial \alpha}\right)^2\left(\frac{\delta\alpha}{\alpha}\right)^2 + (\beta)^2\left(\frac{\partial P}{\partial \beta}\right)^2\left(\frac{\delta\beta}{\beta}\right)^2 + (\gamma)^2\left(\frac{\partial P}{\partial \gamma}\right)^2\left(\frac{\delta\gamma}{\gamma}\right)^2 + (E)^2\left(\frac{\partial P}{\partial E}\right)^2\left(\frac{\delta E}{E}\right)^2 + (ZPV_{cal})^2\left(\frac{\partial P}{\partial ZPV_{cal}}\right)^2\left(\frac{\delta ZPV_{cal}}{ZPV_{cal}}\right)^2 + (ZPV_{flt})^2\left(\frac{\partial P}{\partial ZPV_{flt}}\right)^2\left(\frac{\delta ZPV_{flt}}{ZPV_{flt}}\right)^2\right]^{\frac{1}{2}} \quad (22)$$

and with substitution we get

$$(\alpha)^2\left(\frac{\partial P}{\partial \alpha}\right)^2 = (\alpha)^2,$$
$$(\beta)^2\left(\frac{\partial P}{\partial \beta}\right)^2 = [\beta(E + ZPV_{cal} - ZPV_{flt})]^2,$$
$$(\gamma)^2\left(\frac{\partial P}{\partial \gamma}\right)^2 = (\gamma)^2(E + ZPV_{cal} - ZPV_{flt})^4,$$
$$(E)^2\left(\frac{\partial P}{\partial E}\right)^2 = \{E[\beta + 2\gamma(E + ZPV_{cal} - ZPV_{flt})]\}^2,$$
$$(ZPV_{cal})^2\left(\frac{\partial P}{\partial ZPV_{cal}}\right)^2 = \{ZPV_{cal}[\beta + 2\gamma(E + ZPV_{cal} - ZPV_{flt})]\}^2,$$
$$(ZPV_{flt})^2\left(\frac{\partial P}{\partial ZPV_{flt}}\right)^2 = \{ZPV_{flt}[\beta + 2\gamma(E + ZPV_{cal} - ZPV_{flt})]\}^2.$$

The expression for the uncertainty in the measured pressure, δP, can now be given in its final form as

$$\delta P = \Bigg[(\alpha)^2\left(\frac{\delta\alpha}{\alpha}\right)^2 + [\beta(E + ZPV_{cal} - ZPV_{flt})]^2\left(\frac{\delta\beta}{\beta}\right)^2 + (\gamma)^2[E + ZPV_{cal} - ZPV_{flt}]^4\left(\frac{\delta\gamma}{\gamma}\right)^2 + \{E[\beta + 2\gamma(E + ZPV_{cal} - ZPV_{flt})]\}^2\left(\frac{\delta E}{E}\right)^2 + \{ZPV_{cal}[\beta + 2\gamma(E + ZPV_{cal} - ZPV_{flt})]\}^2\left(\frac{\delta ZPV_{cal}}{ZPV_{cal}}\right)^2 + \{ZPV_{flt}[\beta + 2\gamma(E + ZPV_{cal} - ZPV_{flt})]\}^2\left(\frac{\delta ZPV_{flt}}{ZPV_{flt}}\right)^2\Bigg]^{\frac{1}{2}} \quad (23)$$

XI. ERROR ANALYSIS OF AIR FLOW RATE

The basic calibration equation results from a second order least squares curve fit of pressure on gauge output voltage, i.e.,

$$F_{air} = A + B(\Delta P^2) + C(\Delta P^2)^2 \tag{24}$$

where

$$\Delta P^2 = P_t{}^2 - P_C{}^2$$

with P_t and P_C defined to be the entrance port pressure and the reaction chamber pressure respectively. We can expand equation (24)

$$F_{air} = A + B(P_t{}^2 - P_C{}^2) + C(P_t{}^2 - P_C{}^2)^2 \tag{25}$$

with the variables

A, B, C, P_t, and P_C.

along with the corresponding uncertainties

δA, δB, δC, δP_t, and δP_C.

The uncertainty in the calculated flow rate of air through the inlet let flow tube as a function of the uncertainty in the variables can be expressed as

$$\delta F_{air} = \left[\left(\frac{\partial F_{air}}{\partial A}\right)^2(\delta A)^2 + \left(\frac{\partial F_{air}}{\partial B}\right)^2(\delta B)^2 + \left(\frac{\partial F_{air}}{\partial C}\right)^2(\delta C)^2 + \left(\frac{\partial F_{air}}{\partial P_t}\right)^2(\delta P_t)^2 + \left(\frac{\partial F_{air}}{\partial P_C}\right)^2(\delta P_C)^2\right]^{\frac{1}{2}} \tag{26}$$

The partial derivatives in terms of the variables from equation (24) are:

$$\frac{\partial F_{air}}{\partial A} = 1,$$
$$\frac{\partial F_{air}}{\partial B} = P_t{}^2 + P_C{}^2,$$
$$\frac{\partial F_{air}}{\partial C} = (P_t{}^2 - P_C{}^2)^2,$$
$$\frac{\partial F_{air}}{\partial P_t} = 2P_t[B + 2C(P_t{}^2 - P_C{}^2)],$$
$$\frac{\partial F_{air}}{\partial P_C} = -2P_C[B + 2C(P_t{}^2 - P_C{}^2)].$$

Now equation (26) can be rewitten as

$$\delta F_{air} = \left[(A)^2\left(\frac{\partial F_{air}}{\partial A}\right)^2\left(\frac{\delta A}{A}\right)^2 + (B)^2\left(\frac{\partial F_{air}}{\partial B}\right)^2\left(\frac{\delta B}{B}\right)^2 + (C)^2\left(\frac{\partial F_{air}}{\partial C}\right)^2\left(\frac{\delta C}{C}\right)^2 + (P_t)^2\left(\frac{\partial F_{air}}{\partial P_t}\right)^2\left(\frac{\delta P_t}{P_t}\right)^2 + (P_C)^2\left(\frac{\partial F_{air}}{\partial P_C}\right)^2\left(\frac{\delta P_C}{P_C}\right)^2\right]^{\frac{1}{2}} \quad (27)$$

and with substitution we get

$$(A)^2\left(\frac{\partial F_{air}}{\partial A}\right)^2 = (A)^2,$$

$$(B)^2\left(\frac{\partial F_{air}}{\partial B}\right)^2 = [B(P_t{}^2 - P_C{}^2)]^2,$$

$$(C)^2\left(\frac{\partial F_{air}}{\partial C}\right)^2 = [C(P_t{}^2 - P_C{}^2)^2]^2,$$

$$(P_t)^2\left(\frac{\partial F_{air}}{\partial P_t}\right)^2 = \{2P_t{}^2[B + 2C(P_t{}^2 - P_C{}^2)]\}^2,$$

$$(P_C)^2\left(\frac{\partial F_{air}}{\partial P_C}\right)^2 = \{2P_C{}^2[B + 2C(P_t{}^2 - P_C{}^2)]\}^2.$$

The expression for the uncertainty in the calculated flow rate of air can now be given in its final form as

$$\delta F_{air} = \left[(A)^2\left(\frac{\delta A}{A}\right)^2 + [B(P_t{}^2 - P_C{}^2)]^2\left(\frac{\delta B}{B}\right)^2 + [C(P_t{}^2 - P_C{}^2)^2]^2\left(\frac{\delta C}{C}\right)^2 + \{2P_t{}^2[B + 2C(P_t{}^2 - P_C{}^2)]\}^2\left(\frac{\delta P_t}{P_t}\right)^2 + \{2P_C{}^2[B + 2C(P_t{}^2 - P_C{}^2)]\}^2\left(\frac{\delta P_C}{P_C}\right)^2\right]^{\frac{1}{2}} \quad (28)$$

XII. INSTRUMENT OUTPUT SIGNAL

An example the the phototube output signal for a typical rocket flight is shown in Figure 14. At approximately 225 seconds of elapsed time the reagent gas, containing ozone, is released to flow into the reaction volume. The lower set of data show the resulting signal level that represent the phototube 'dark count', **IB**, plus the ozone generated background signal, **IO**. Each background data point shown in the figure represents the mean value of four 1 second integration periods.

The phototube output signal given by **IT** is the total signal an includes the photons generated in the reaction between NO and O_3. The difference between the two levels, **IS**, gives a direct measure of the nitric oxide mixing ratio if we know the sensitivity of the instrument.

Figure 15 is an example of the instrument sensitivity for one particular rocket flight, NASA 30.027. From section III we found that is is a function of the incomming sample flow rate, the reaction chamber pressure, the reaction chamber temperature, the reagent gas flow rate, and the ozone mixing ratio of the reagent gas.

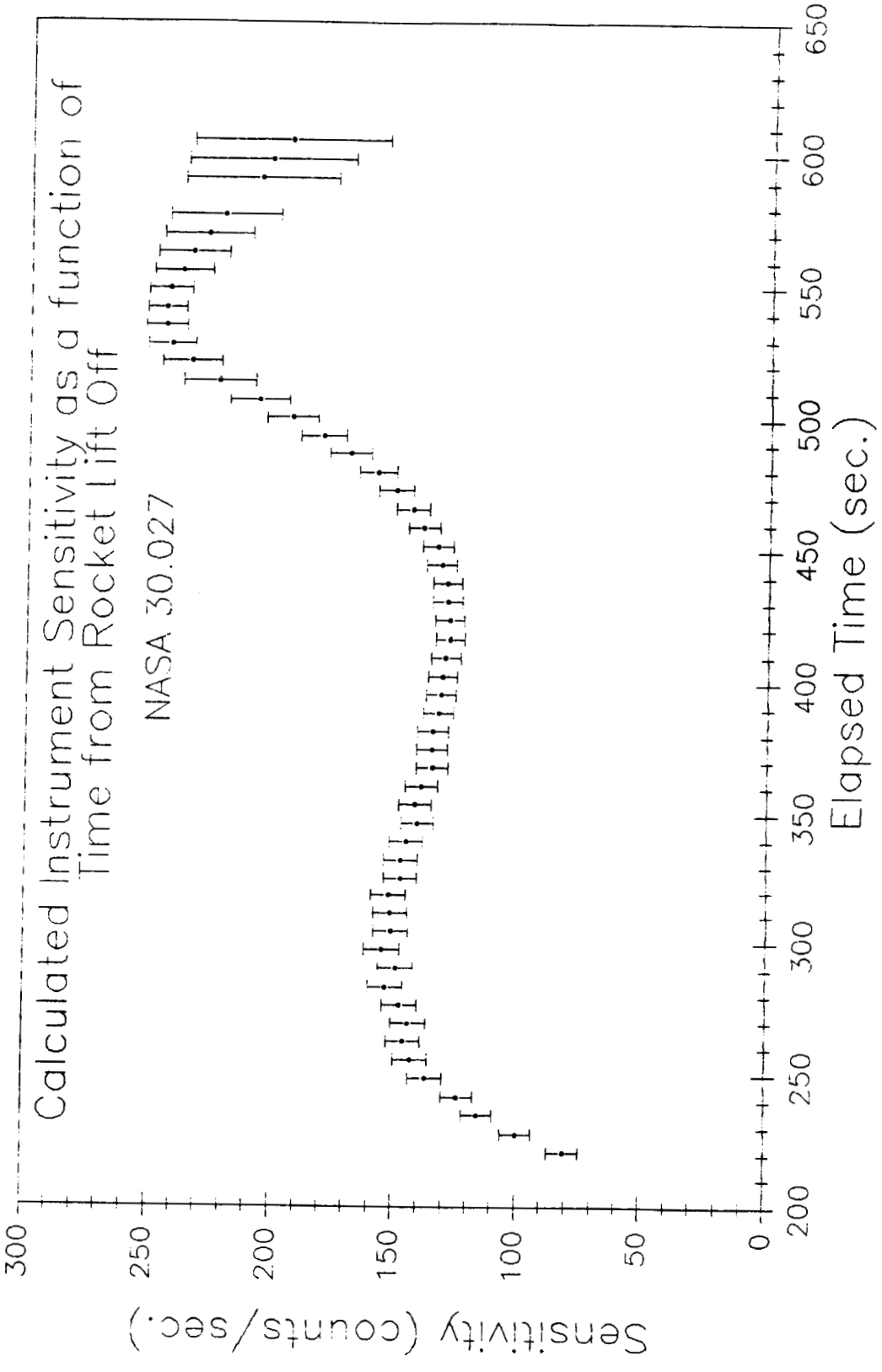

XIII. INITIAL MEASUREMENT RESULTS

Figures 16 through 24 show the results of the initial seven rocket flights for which nitric oxide mixing ratio data were obtained. These flights predated the current NASA grant but are included for completeness.

XIII.a Nasa Payload 15.157

Figure 16 shows the results from the first flight of the first rocket lauched-parchute borne payload flown for the purpose of obtaining the nitric oxide mixing ratio. The rocket type was a boosted Arcas. Because of it's small diameter and payload capability we were constrained in both weight and size. The required use of this vehicle set most of the guidelines for the rest of the measurement program. For example we used the PSL Arcas type telemtry throughout the entire program. This first launch was unique in that we used the boil off from the LN_2 cryopump as a source for the background bias flow gas. For the most part it appeared to be successful except, as we will find later, nitrogen does not have the same quenching properties as oxygen and the measured background signal is too large,i.e., the resulting mixing ratio will have been too low over at least some part of the altitude range. These data are not corrected for errors due to a nitrogen bias gas.

XIII.b Nasa Payload 23.011

Figure 17 shows the results of the first payload that was launched by an Astrobee-D rocket. The increased diameter and launch weight capability permitted an itteration in the payload design. We increased the weight from 5.9 kg.(13 lb.) to approx. 9.5 kg(21 lb). and were able to expand the diameter of the electronics section. The most important iteration, however, was the ability to carry an onboard supply of pressurized nitrogen to use for the background bias gas. Again, this turned out to be an unfortunent choice. The experiment worked fine but the rocket range could not provide a current measurement of the atmospheric parameters, i.e., profiles of pressure, temperature, or density. Since this payload was not instrumented with a pressure gauge for the measurement of the stagnation pressure, we were forced to estimate the pressure environment. the relatively large error bars on the data are caused by this problem. These data have not been corrected for errors due to a nitrogen bias gas.

XIII.c Nasa Payload 23.013

Figure 18 Shows a foreshortened nitric oxide profile. The asbestos phenelic nosecone shroud failed to eject until just over 36 km. Ozone was entering continuously into the reaction volume for a period of approximately 100 seconds. These data should not be considered for scientific purposes but we did get some engineering information that was useful. We found that the amount of nitric oxide lost in the free stream as a result of having ozone migrate upstream of the reaction volume, i.e., having it get into the inlet tube as it did here, was closely related to the time exposure ozne in the tube and the

flow rate of the incomming sample gas. Even though the inlet tube was exposed to a large dose of ozone for a long period of time the large flow rates at the lower altitudes inhibit the loss of NO molecules. These data have not been corrected for errors due to a nitrogen bias gas.

XIII.d Nasa Flight 23.014

The results in Figure 19 show the beginning of a seemingly benign problem associated with the desire to extend the measurement range to higher altitudes. As we observe their is a negative slope to the data above 38 km. This same tendency will be found in several of the following data sets. We did not recognize the problem until the flight of Nasa 30.004. It was related to ozone migrating into the inlet tube. The relatively large flow rate of the reagent gas that was used during those launches, approx. 0.6 cc/s(NTP), increased the reaction chamber pressure just enough to cause a reverse flow rate at the upper altitude limit. Although the upper altitude profile is not representative of the actual NO profile our subsequent laboratory experiments show that the profiles should not be affected below approximately 45 km. Again, these data have not been corrected for errors due to a nitrogen bias gas.

XIII.e Nasa Flight 23.015

The comments for Figure 20 are the same as Figure 19. These data have not been corrected for errors due to a nitrogen bias gas.

XIII.f Nasa Flight 30.003

The comments for Figure 21 are the same as Figure 19. The rocket used with this experiment was upgraded to a Sparrow. The Sparrow rocket is a 14 in diameter vehicle that has dual thrust. The prior Astrobee-D nose cone design was adapted to the Sparrow by a 5.5 degree half angle conical shroud. All subsequent rocket launches included the use of the Sparrow rocket. No other significant changes were made to the payload at this time. These data have not been corrected for errors due to a nitrogen bias gas.

XIII.g Nasa Flight 30.004

The comments for Figure 22 are the same as Figure 19. These data have not been corrected for errors due to a nitrogen bias gas.

XIII.h Nasa Flight 30.008

The comments for Figure 23 are the same as Figure 19. It should be noted this was the second launch of two launches to take place on 23 July 1981. (See Figure 24) The purpose was to investigate the repeatability of the measurement technique. Even though we has already identified the ozone contamination problem before these flights the valve

timer malfunctioned and released the reagent gas 15 seconds early. Comparison with Nasa Flight 30.014 shows a discrepancy, between data sets, above approximately 44 km.

It should be noted that the error bars have been significantly reduced with this flight. We have finally introduced a pressure measurement at the entrance to the inlet flow tube. This enables us to determine the air flow rate independently, and with higher accuracy. These data have not been corrected for errors due to a nitrogen bias gas.

XIII.i Nasa Flight 30.014

The results shown in Figure 24 shows the first signifcant high altitude profile of the nitric oxide mixing ratio. We reduced the reagent gas flow rate, such that the effective reaction chamber pressure would be somewhat lower in order to minimize the ozone contamination problem. (We really did not identifiy th ozone contamination problem until we installed the second pressure gauge at the inlet side of the inlet flow tube.) These data have not been corrected for errors due to a nitrogen bias gas.

A comparison of data between the two rocket launches was very good below 45 km in altitude. In spite of the nitrogen bias gas problem that we were not aware of at this point the repeatability of the data was excellent. This repeatability caused us to be too secure in our observation of the data sets.

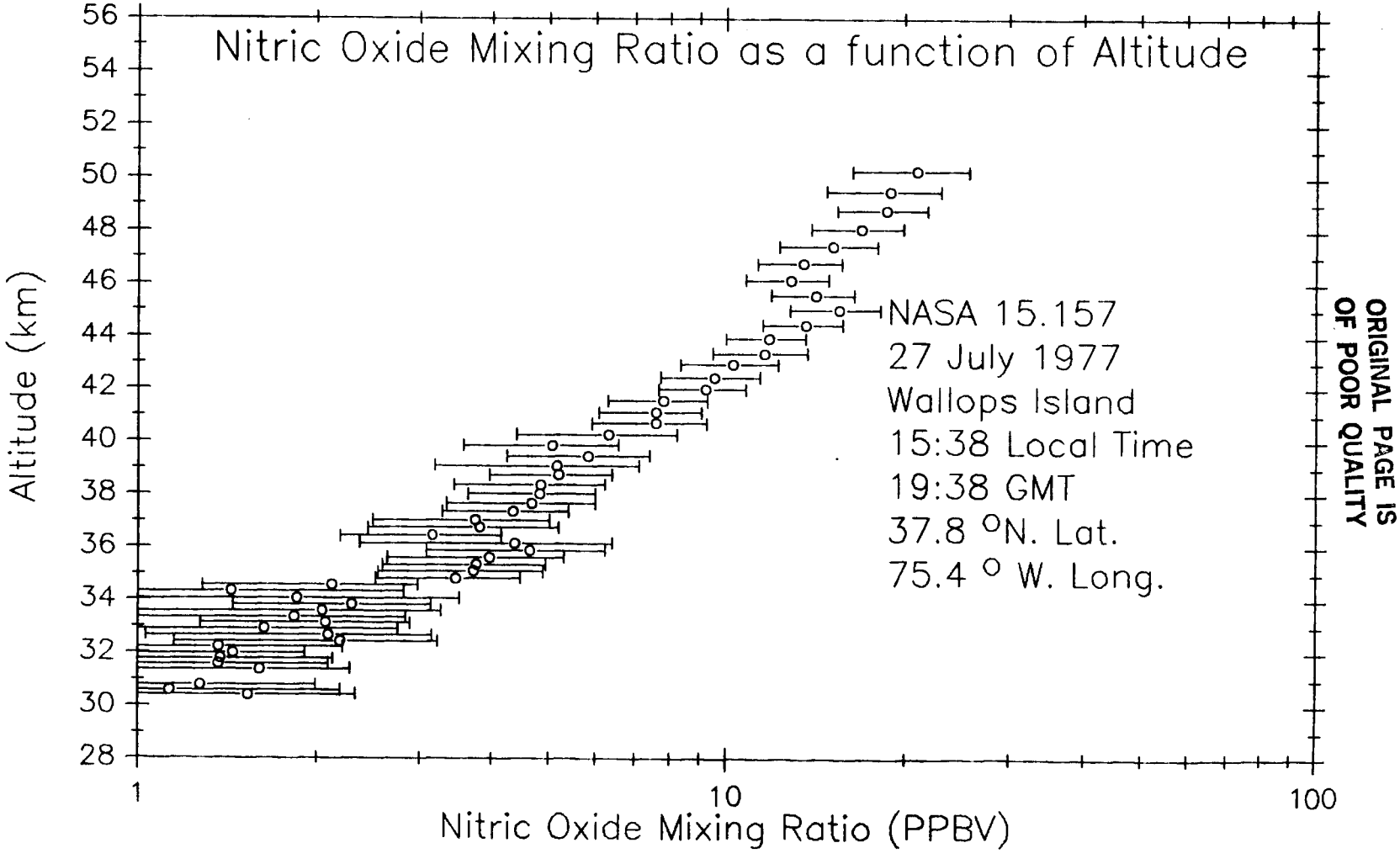

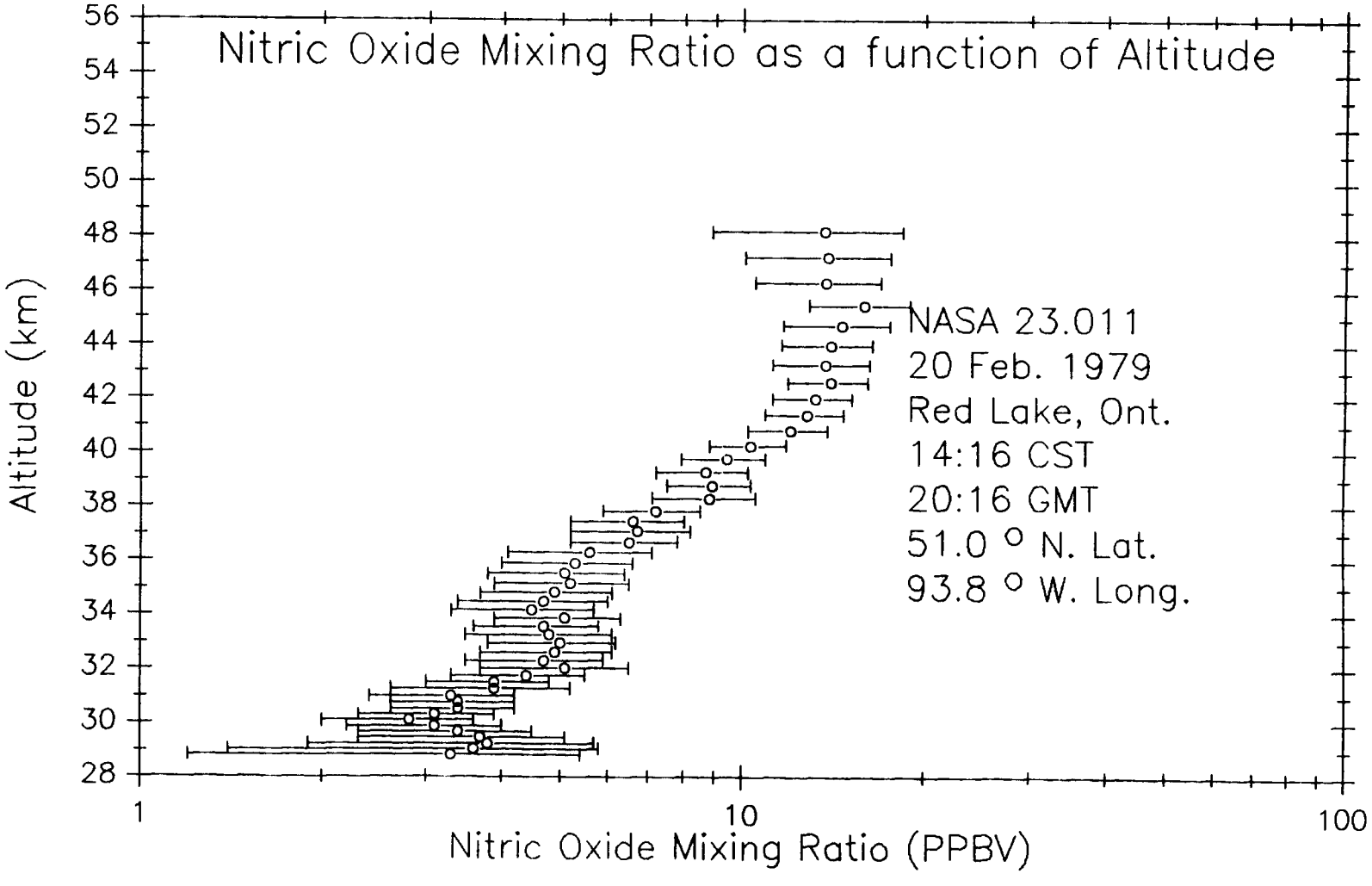
Nitric Oxide Mixing Ratio as a function of Altitude
Altitude (km)
56
54
52
50
48
46
44
42
40
38
36
34
32
30
28
1
10
100
Nitric Oxide Mixing Ratio (PPBV)
NASA 23.011
20 Feb. 1979
Red Lake, Ont.
14:16 CST
20:16 GMT
51.0 ° N. Lat.
93.8 ° W. Long.

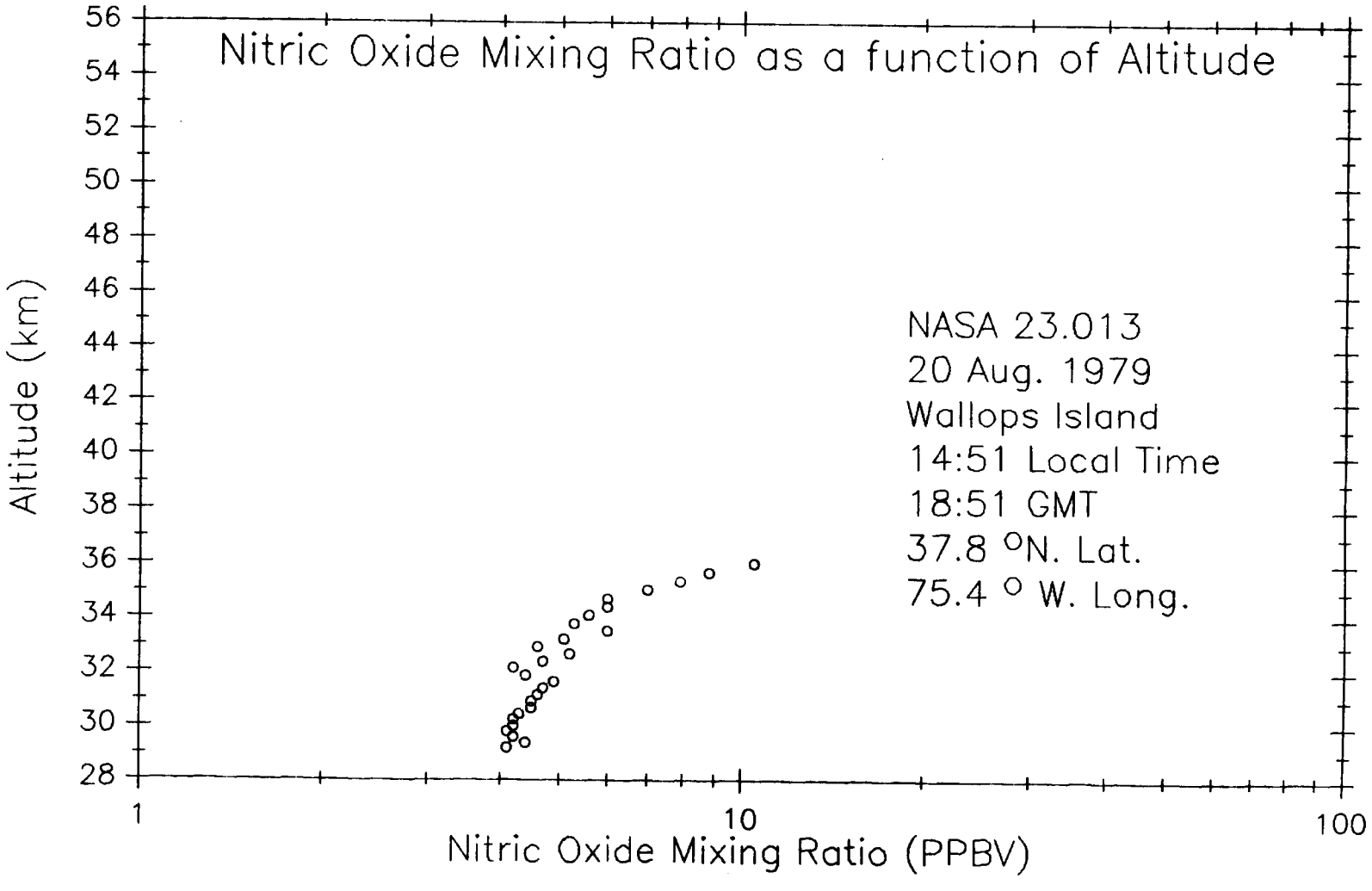
Nitric Oxide Mixing Ratio as a function of Altitude
NASA 23.013
20 Aug. 1979
Wallops Island
14:51 Local Time
18:51 GMT
37.8 °N. Lat.
75.4 ° W. Long.
Altitude (km)
56
54
52
50
48
46
44
42
40
38
36
34
32
30
28
1
10
100
Nitric Oxide Mixing Ratio (PPBV)

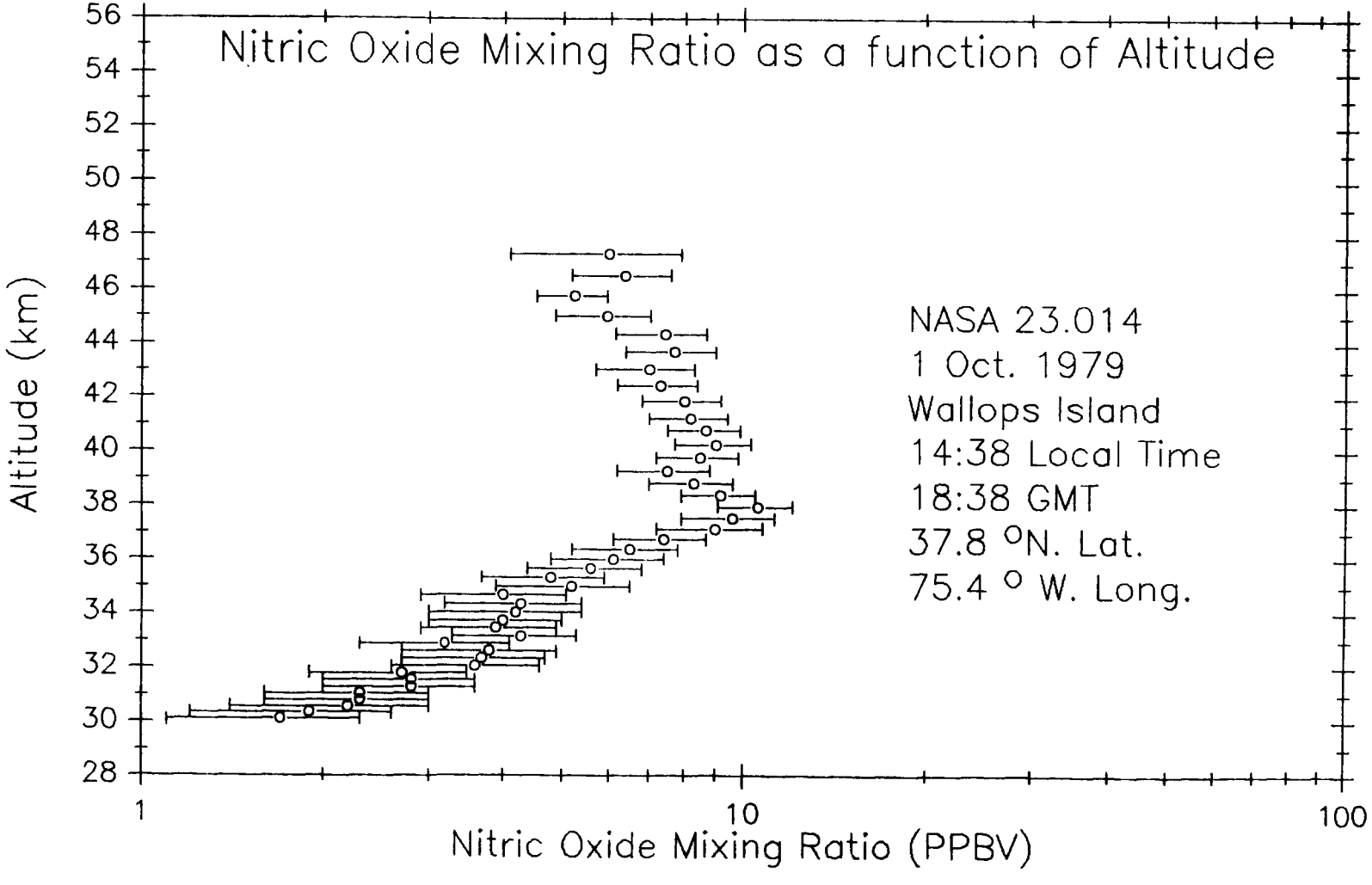
Nitric Oxide Mixing Ratio as a function of Altitude
NASA 23.014
1 Oct. 1979
Wallops Island
14:38 Local Time
18:38 GMT
37.8 °N. Lat.
75.4 ° W. Long.
Altitude (km)
56
54
52
50
48
46
44
42
40
38
36
34
32
30
28
1
10
100
Nitric Oxide Mixing Ratio (PPBV)

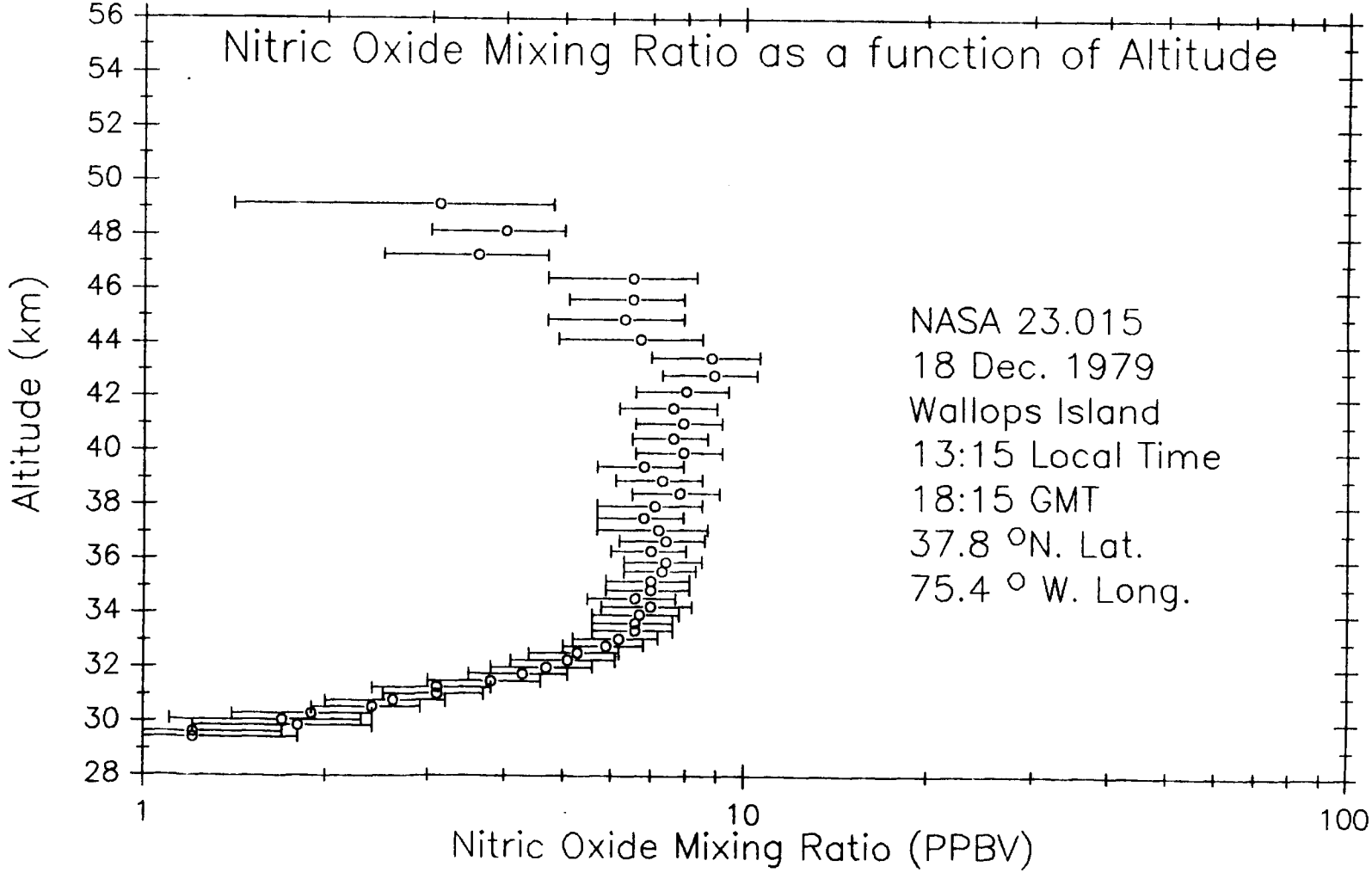
Nitric Oxide Mixing Ratio as a function of Altitude
Altitude (km)
56
54
52
50
48
46
44
42
40
38
36
34
32
30
28
1
10
100
Nitric Oxide Mixing Ratio (PPBV)
NASA 23.015
18 Dec. 1979
Wallops Island
13:15 Local Time
18:15 GMT
37.8 °N. Lat.
75.4 ° W. Long.

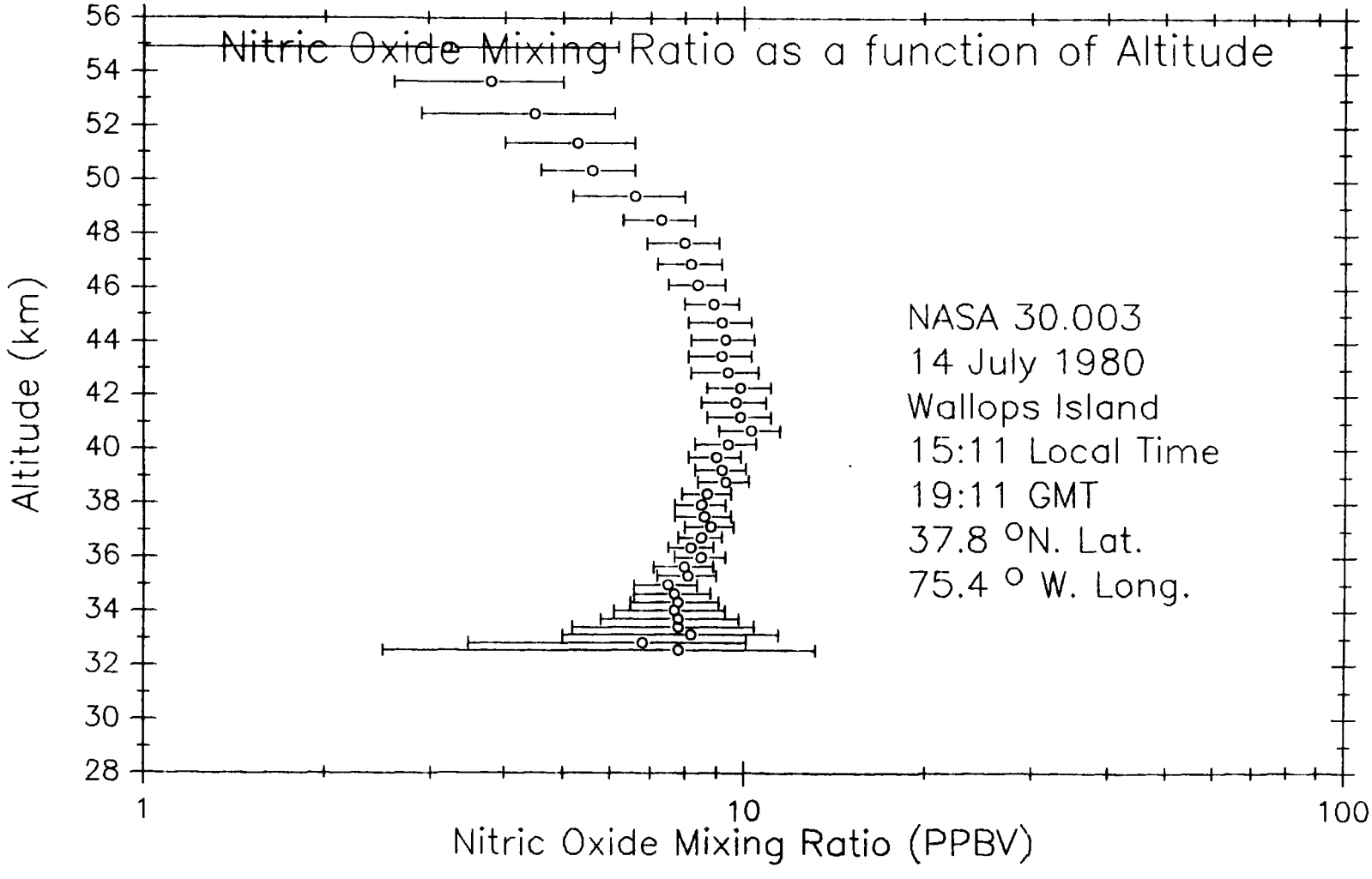
Nitric Oxide Mixing Ratio as a function of Altitude
NASA 30.003
14 July 1980
Wallops Island
15:11 Local Time
19:11 GMT
37.8 °N. Lat.
75.4 ° W. Long.
Altitude (km)
56
54
52
50
48
46
44
42
40
38
36
34
32
30
28
1
10
100
Nitric Oxide Mixing Ratio (PPBV)

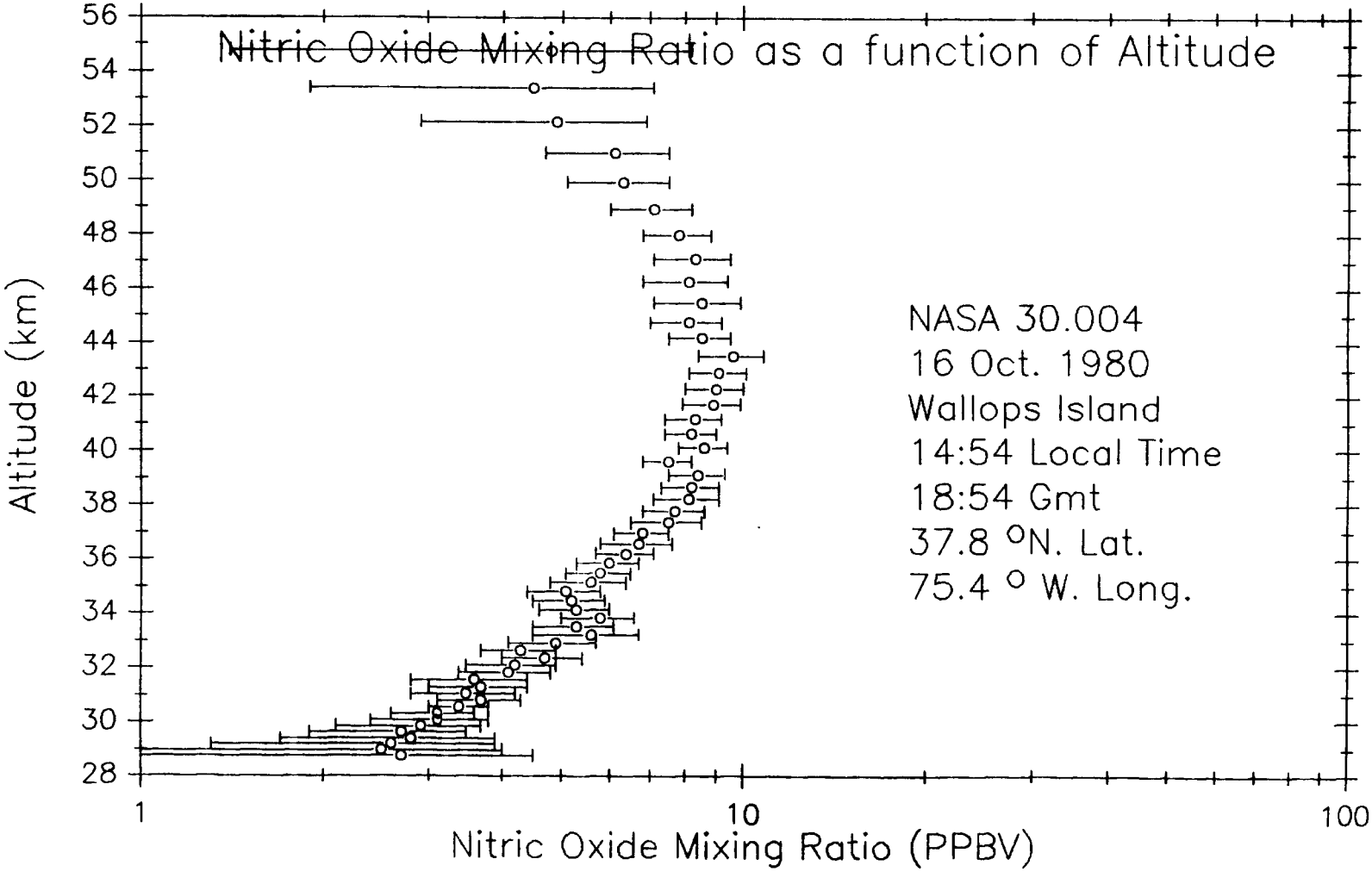
Nitric Oxide Mixing Ratio as a function of Altitude
NASA 30.004
16 Oct. 1980
Wallops Island
14:54 Local Time
18:54 Gmt
37.8 °N. Lat.
75.4 ° W. Long.
Altitude (km)
56
54
52
50
48
46
44
42
40
38
36
34
32
30
28
1
10
100
Nitric Oxide Mixing Ratio (PPBV)

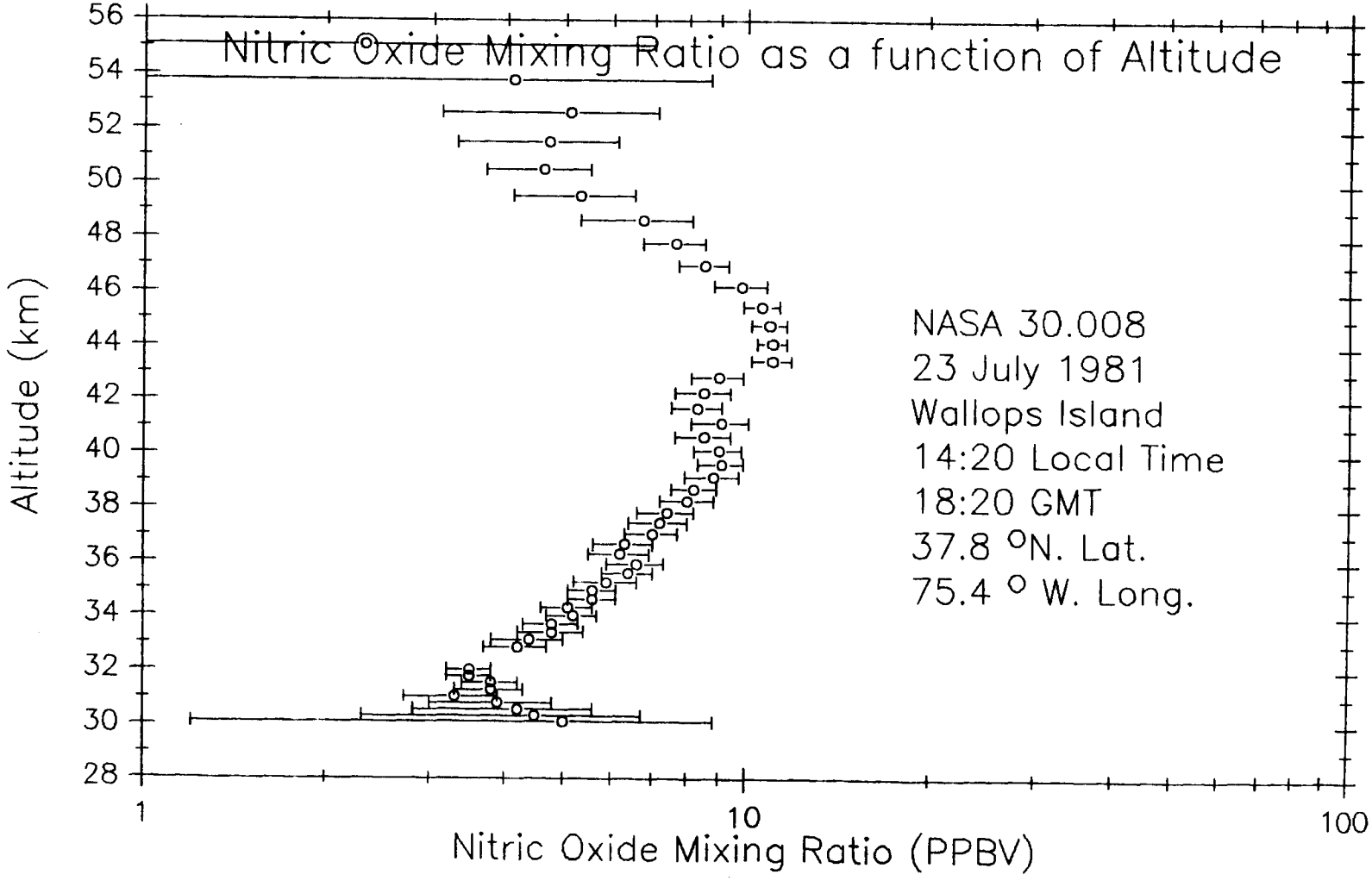
Nitric Oxide Mixing Ratio as a function of Altitude
Altitude (km)
56
54
52
50
48
46
44
42
40
38
36
34
32
30
28
1
10
100
Nitric Oxide Mixing Ratio (PPBV)
NASA 30.008
23 July 1981
Wallops Island
14:20 Local Time
18:20 GMT
37.8 °N. Lat.
75.4 ° W. Long.

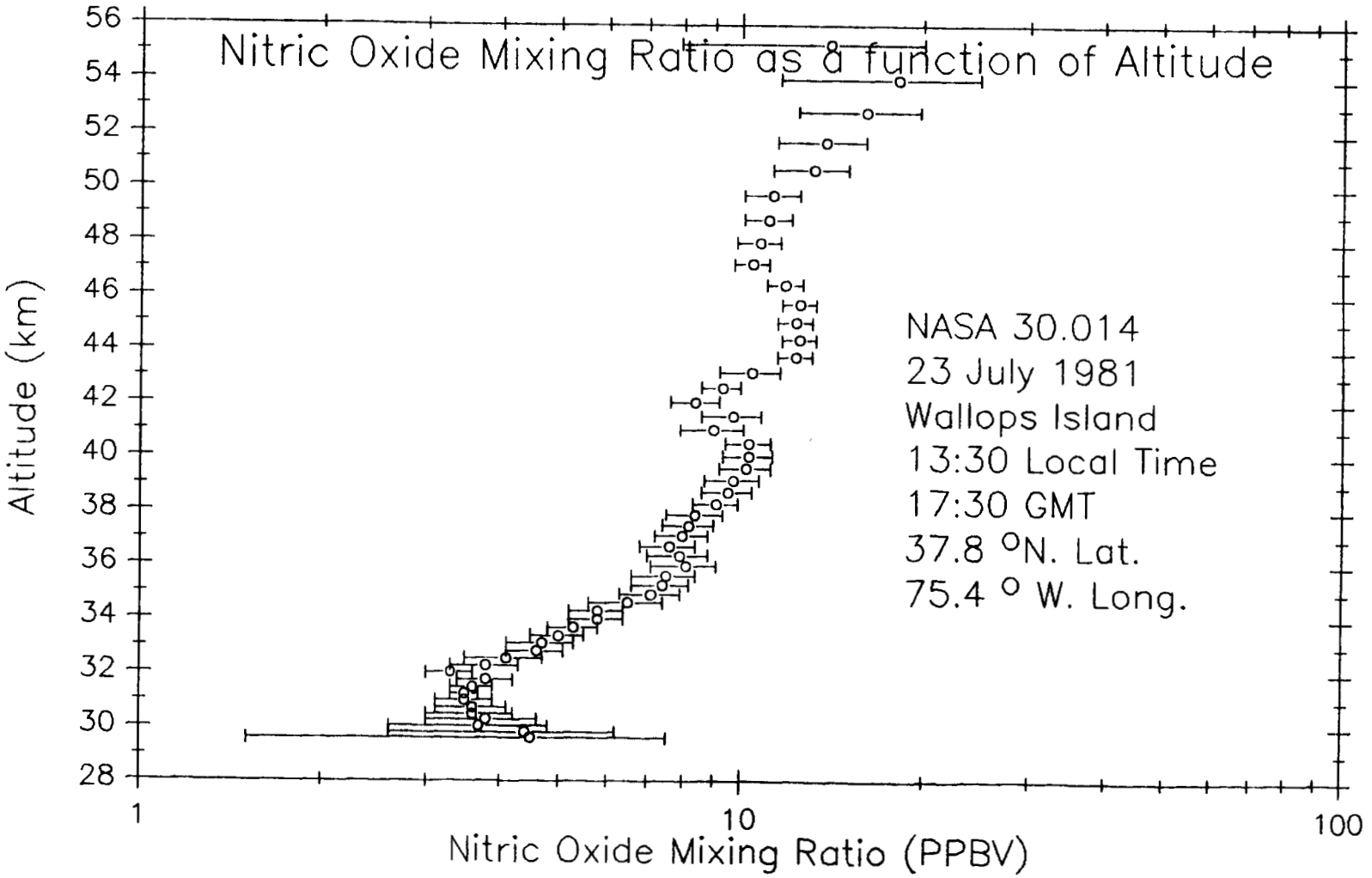
Nitric Oxide Mixing Ratio as a function of Altitude
NASA 30.014
23 July 1981
Wallops Island
13:30 Local Time
17:30 GMT
37.8 °N. Lat.
75.4 ° W. Long.
Altitude (km)
56
54
52
50
48
46
44
42
40
38
36
34
32
30
28
1
10
100
Nitric Oxide Mixing Ratio (PPBV)

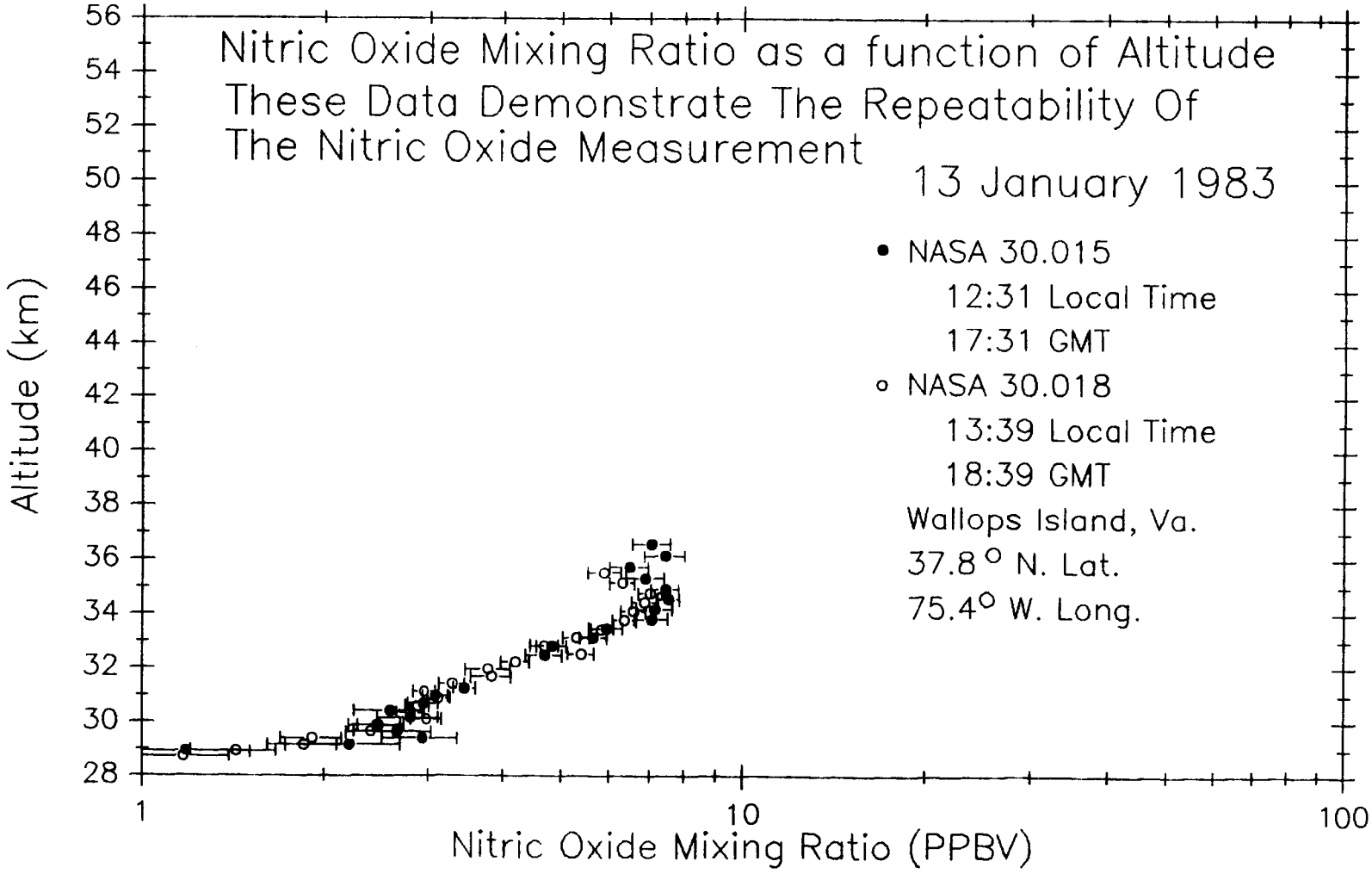
Nitric Oxide Mixing Ratio as a function of Altitude
These Data Demonstrate The Repeatability Of
The Nitric Oxide Measurement
13 January 1983
• NASA 30.015
12:31 Local Time
17:31 GMT
∘ NASA 30.018
13:39 Local Time
18:39 GMT
Wallops Island, Va.
37.8° N. Lat.
75.4° W. Long.
Altitude (km)
56
54
52
50
48
46
44
42
40
38
36
34
32
30
28
1
10
100
Nitric Oxide Mixing Ratio (PPBV)

XIV. CURRENT MEASUREMENT RESULTS

A total of six nitric oxide payloads were launched under the current NASA grant. The first pair, NASA 30.015 and NASA 30.018, were launched at Wallops Island, Va. on 13 Jan. 1983 for the purpose of investigating instrument repeatability. NASA 30.015 contained an inflight calibration capability. We will see that the inflight calibration provided the exact same sensitivity as the calculated sensitivity, i.e., the sensitivity calculated from the instrument model.

For the third time we had a failure of the ozone valve electronic circuit and the valve opened near apogee, shortly after parachute ejection. We will see that their is excellent comparison of the resulting profiles below 35 km. It should be noted that both NASA flights 30.015 and 30.018 used the nitrogen bias gas and these data have not been corrected.

The remaining four flights used air for the background calibration measurement. NASA flight 30.019, Figure 28, was launched at the Poker Flat Rocket Range on 16 August 1984. It was the first launch of a series of three to determine something about the seasonal variation of the nitric oxide mixing ratio at a high latitude site. These data show a very low mixing ratio all the way up to 50 km. No corrections have to be made on these data.

NASA flights 30.023 and 30.024 (Figures 29 and 30) were launched during the following winter at the Poker Flat facility. The 25 Jan. 1985 flight did not start at a high enough altitude to measure the expected high NO mixing ratios. However, the 7 Feb. 1985 flight measured 148 PPBV at 52 km even though the upper stratospheric NO mixing ratio is generally quite low in comparison to the mid-latitude numbers. It should be noted that there was some intense magnetic activity in the morning preceeding this launch.

Figure 31 shows the results of NASA flight 30.027 which was carried out at the White Sands Missile Range. It is the only set of data from a mid-latitude launch site that is not subject to the nitrogen bias gas problem. Figure 32 illustrates the comparison between three data sets. NASA flight 30.027 has been reproduced in this figure as a representative mid-latitude nitric oxide mixing ratio profile in the upper stratosphere. The profile to the left is a compilation of all of the prior mid-latitude balloon borne launches, those that need correction due to the nitrogen biaa gas error. Figure 32 also includes the results from the balloon program of Ridley, et-al.

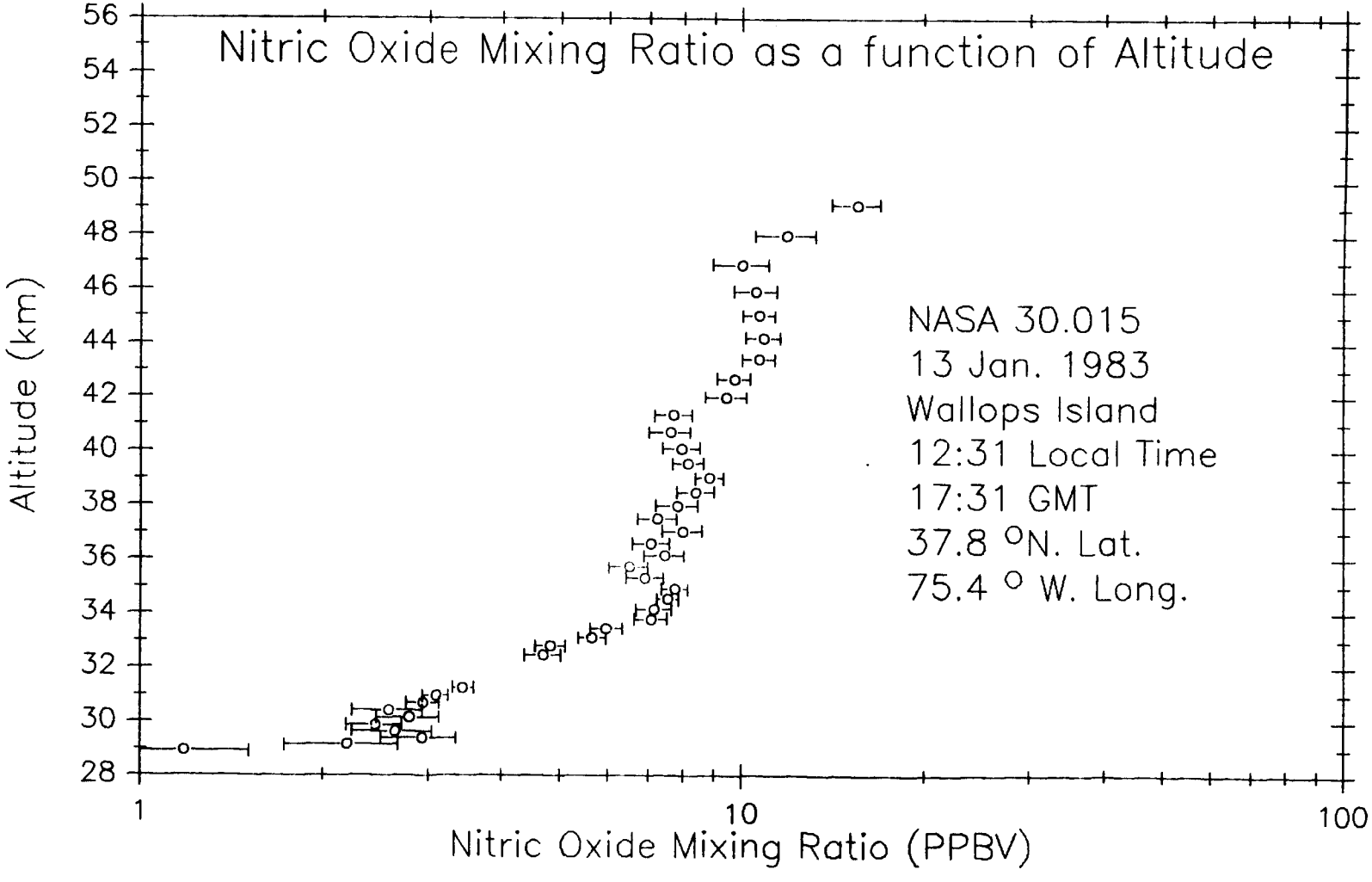
Nitric Oxide Mixing Ratio as a function of Altitude
NASA 30.015
13 Jan. 1983
Wallops Island
12:31 Local Time
17:31 GMT
37.8 °N. Lat.
75.4 ° W. Long.
Altitude (km)
56
54
52
50
48
46
44
42
40
38
36
34
32
30
28
1
10
100
Nitric Oxide Mixing Ratio (PPBV)

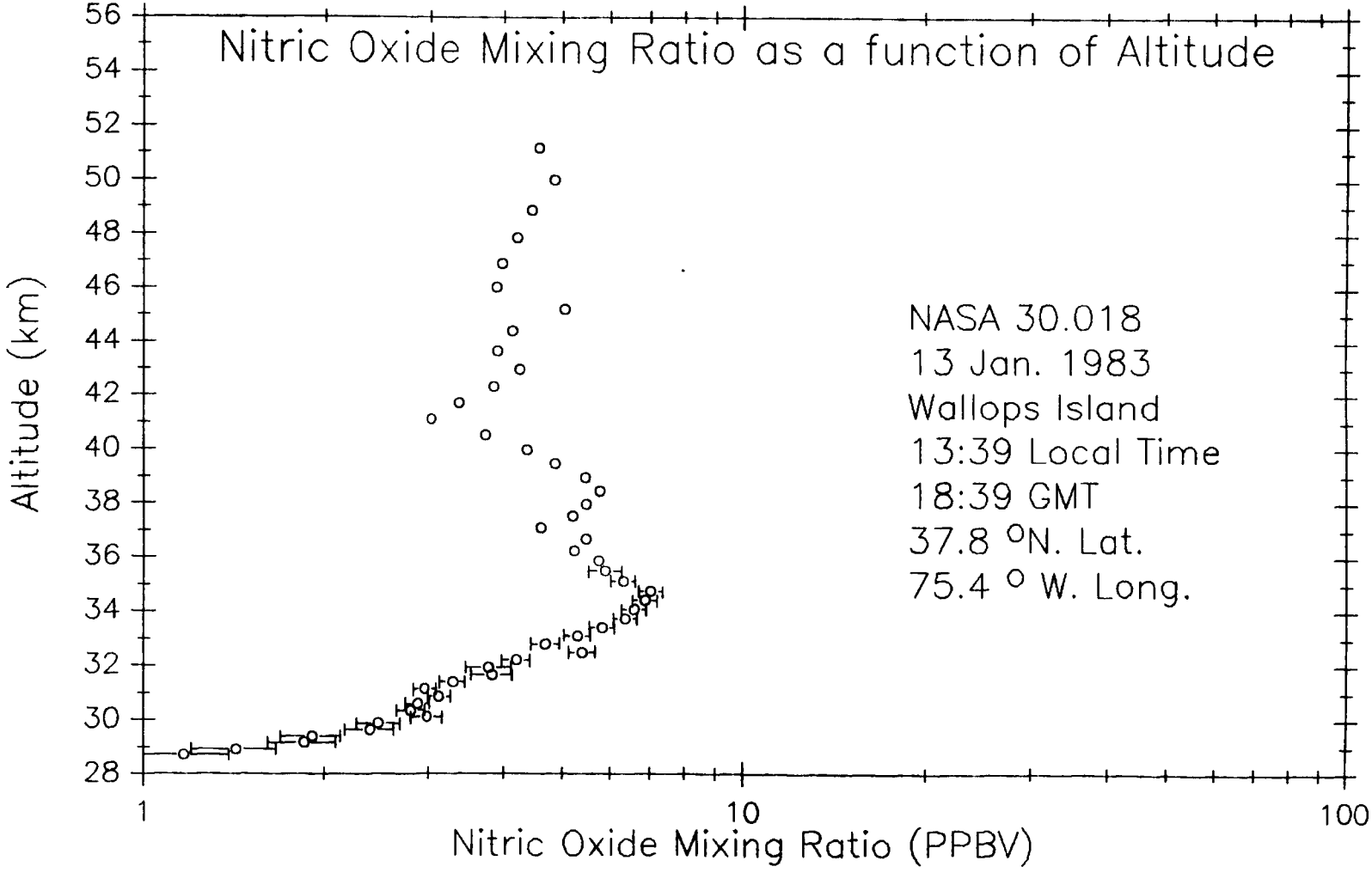
Nitric Oxide Mixing Ratio as a function of Altitude
NASA 30.018
13 Jan. 1983
Wallops Island
13:39 Local Time
18:39 GMT
37.8 °N. Lat.
75.4 ° W. Long.
Altitude (km)
56
54
52
50
48
46
44
42
40
38
36
34
32
30
28
1
10
100
Nitric Oxide Mixing Ratio (PPBV)

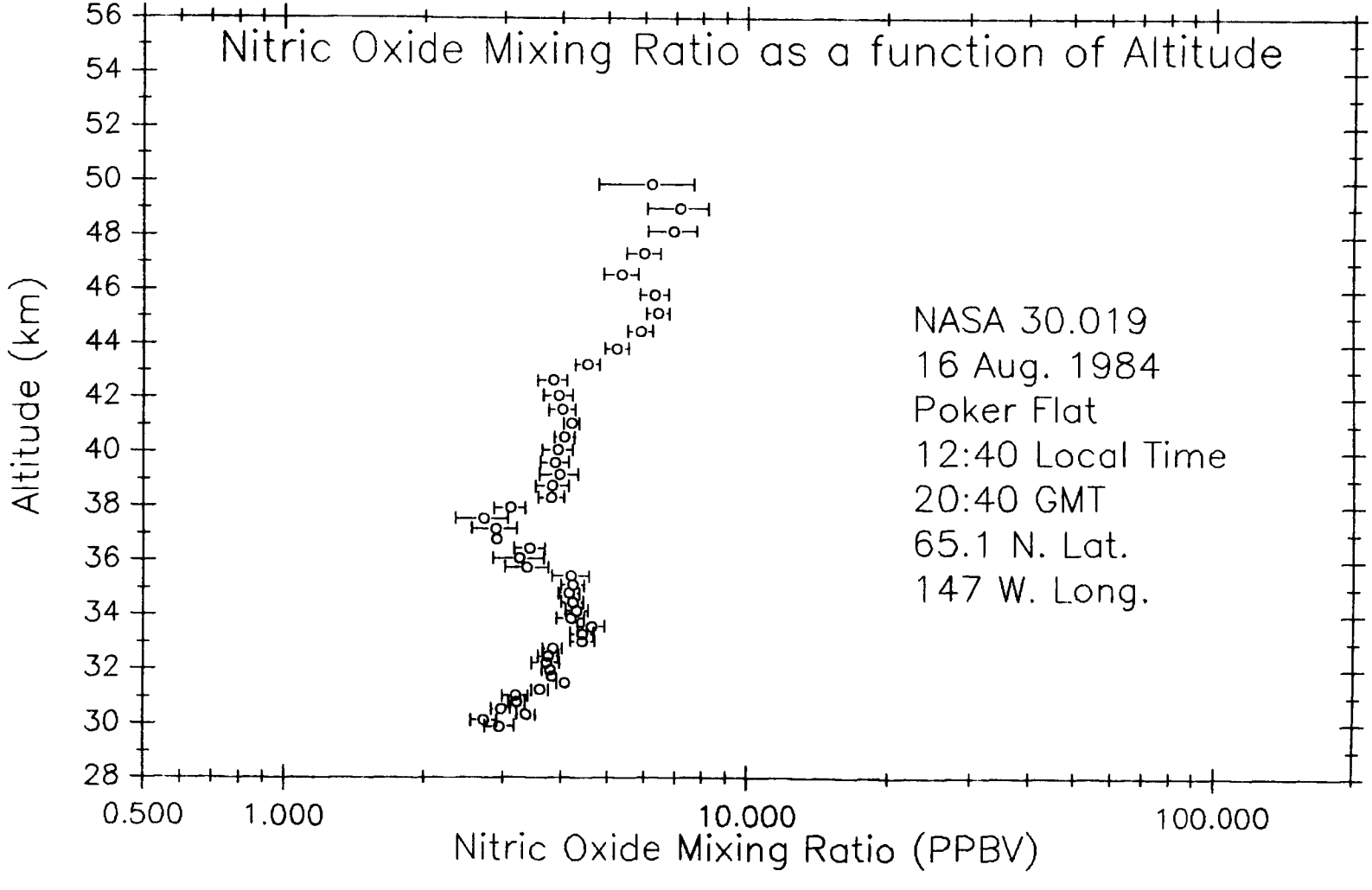
Nitric Oxide Mixing Ratio as a function of Altitude
Altitude (km)
56
54
52
50
48
46
44
42
40
38
36
34
32
30
28
0.500
1.000
10.000
100.000
Nitric Oxide Mixing Ratio (PPBV)
NASA 30.019
16 Aug. 1984
Poker Flat
12:40 Local Time
20:40 GMT
65.1 N. Lat.
147 W. Long.

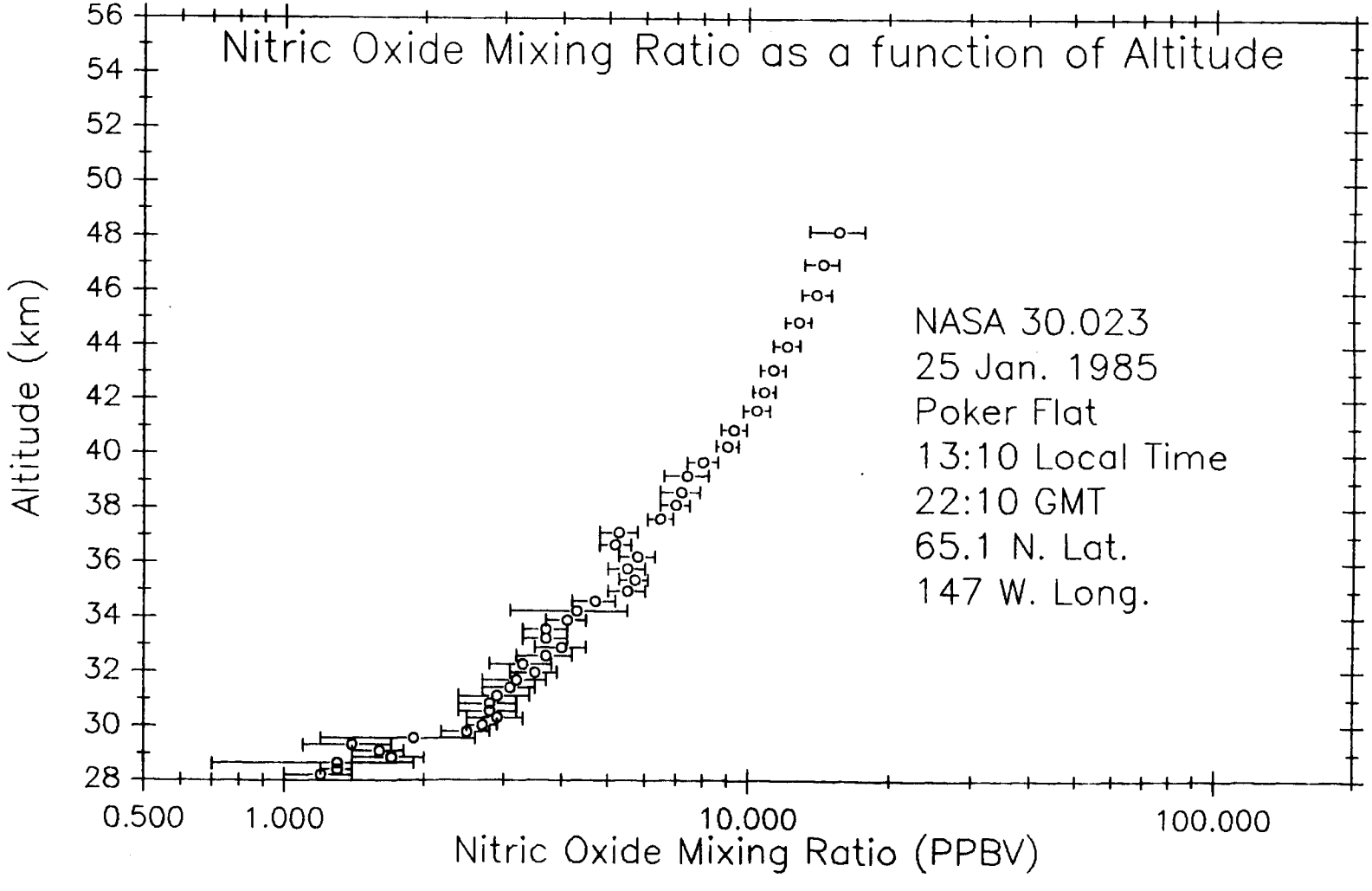
Nitric Oxide Mixing Ratio as a function of Altitude
Altitude (km)
56
54
52
50
48
46
44
42
40
38
36
34
32
30
28
0.500
1.000
10.000
100.000
Nitric Oxide Mixing Ratio (PPBV)
NASA 30.023
25 Jan. 1985
Poker Flat
13:10 Local Time
22:10 GMT
65.1 N. Lat.
147 W. Long.

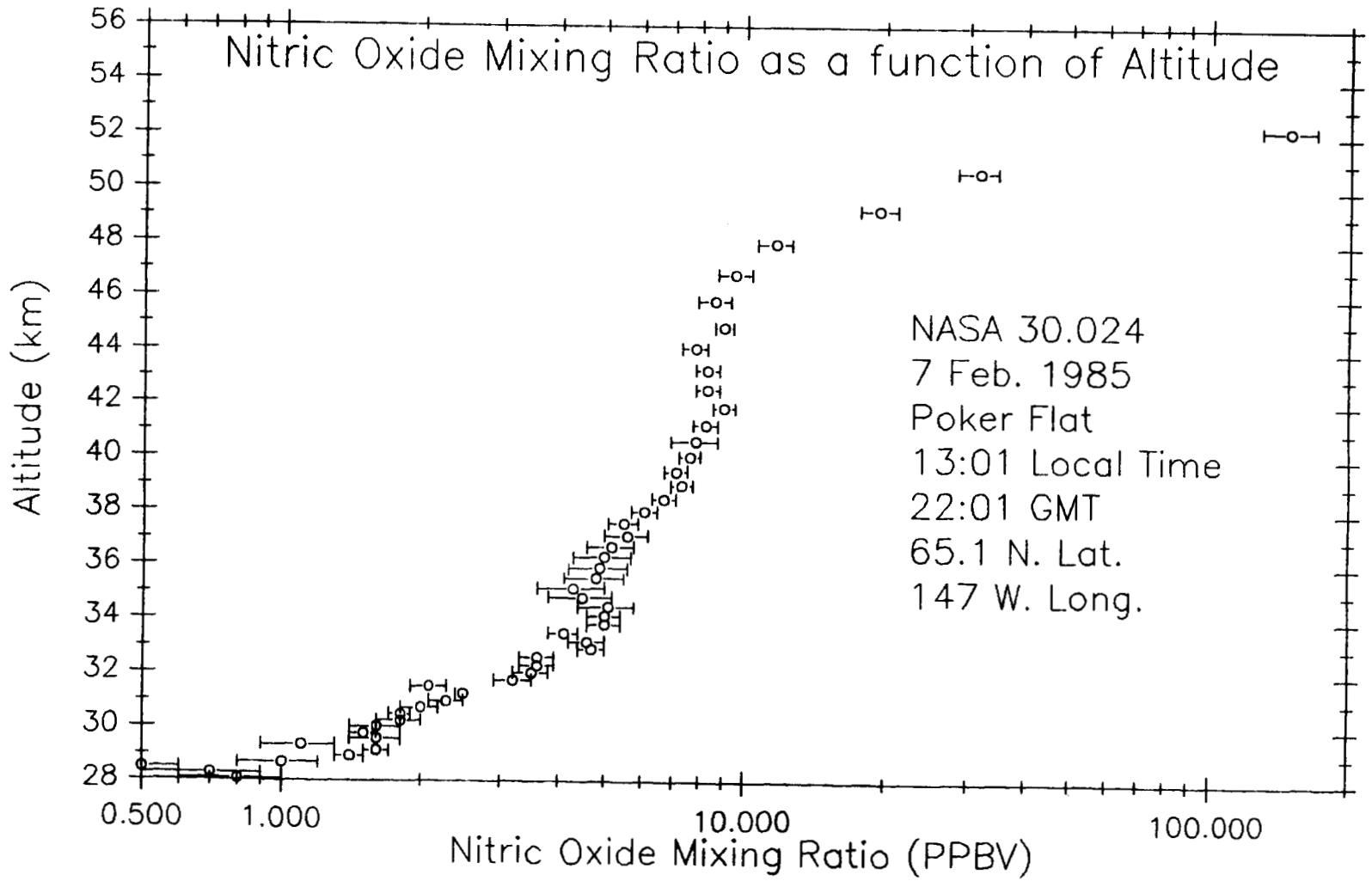
Nitric Oxide Mixing Ratio as a function of Altitude
NASA 30.024
7 Feb. 1985
Poker Flat
13:01 Local Time
22:01 GMT
65.1 N. Lat.
147 W. Long.
Altitude (km)
56
54
52
50
48
46
44
42
40
38
36
34
32
30
28
0.500
1.000
10.000
100.000
Nitric Oxide Mixing Ratio (PPBV)

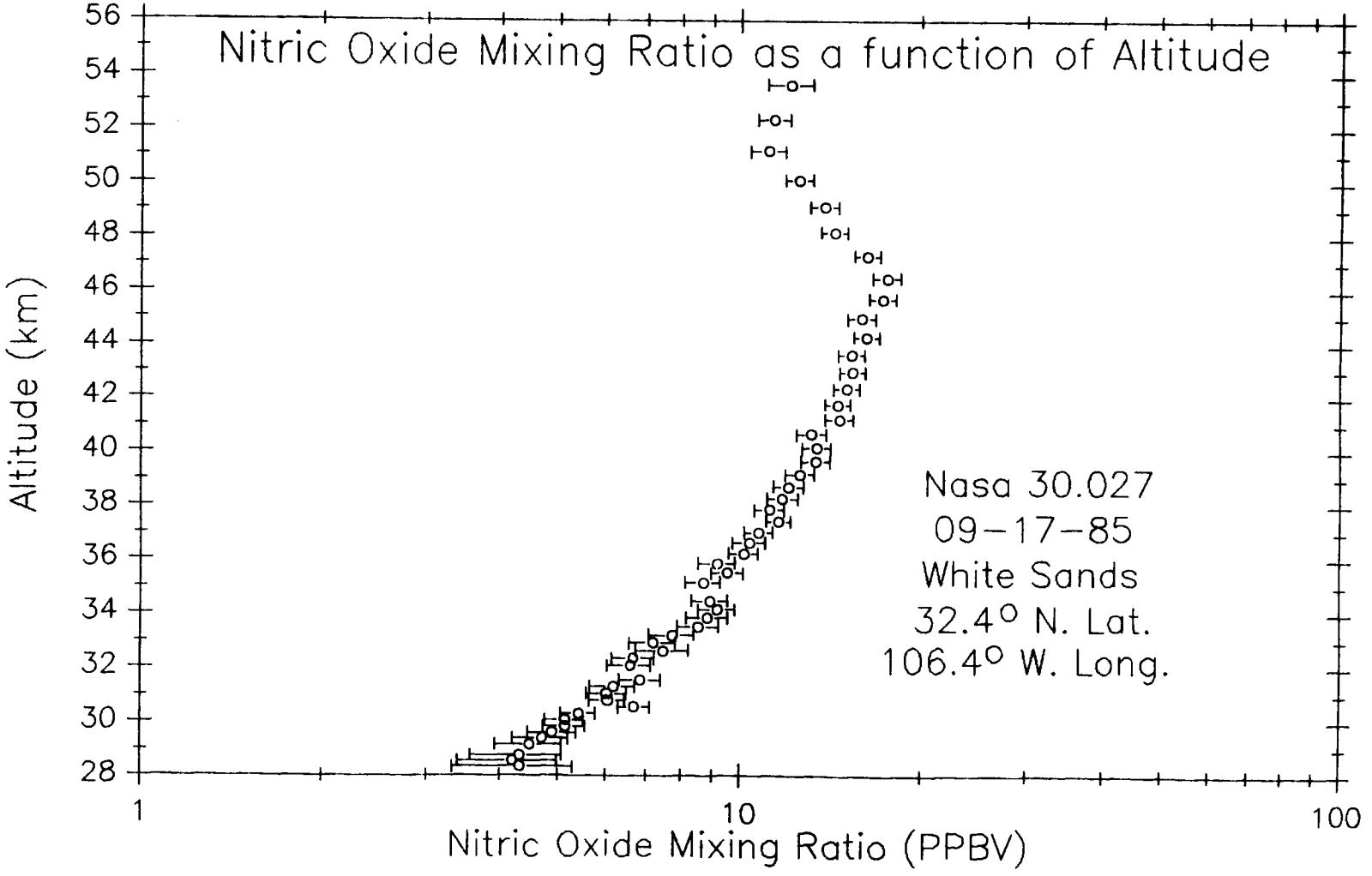
Nitric Oxide Mixing Ratio as a function of Altitude
Altitude (km)
56
54
52
50
48
46
44
42
40
38
36
34
32
30
28
1
10
100
Nitric Oxide Mixing Ratio (PPBV)
Nasa 30.027
09-17-85
White Sands
32.4° N. Lat.
106.4° W. Long.

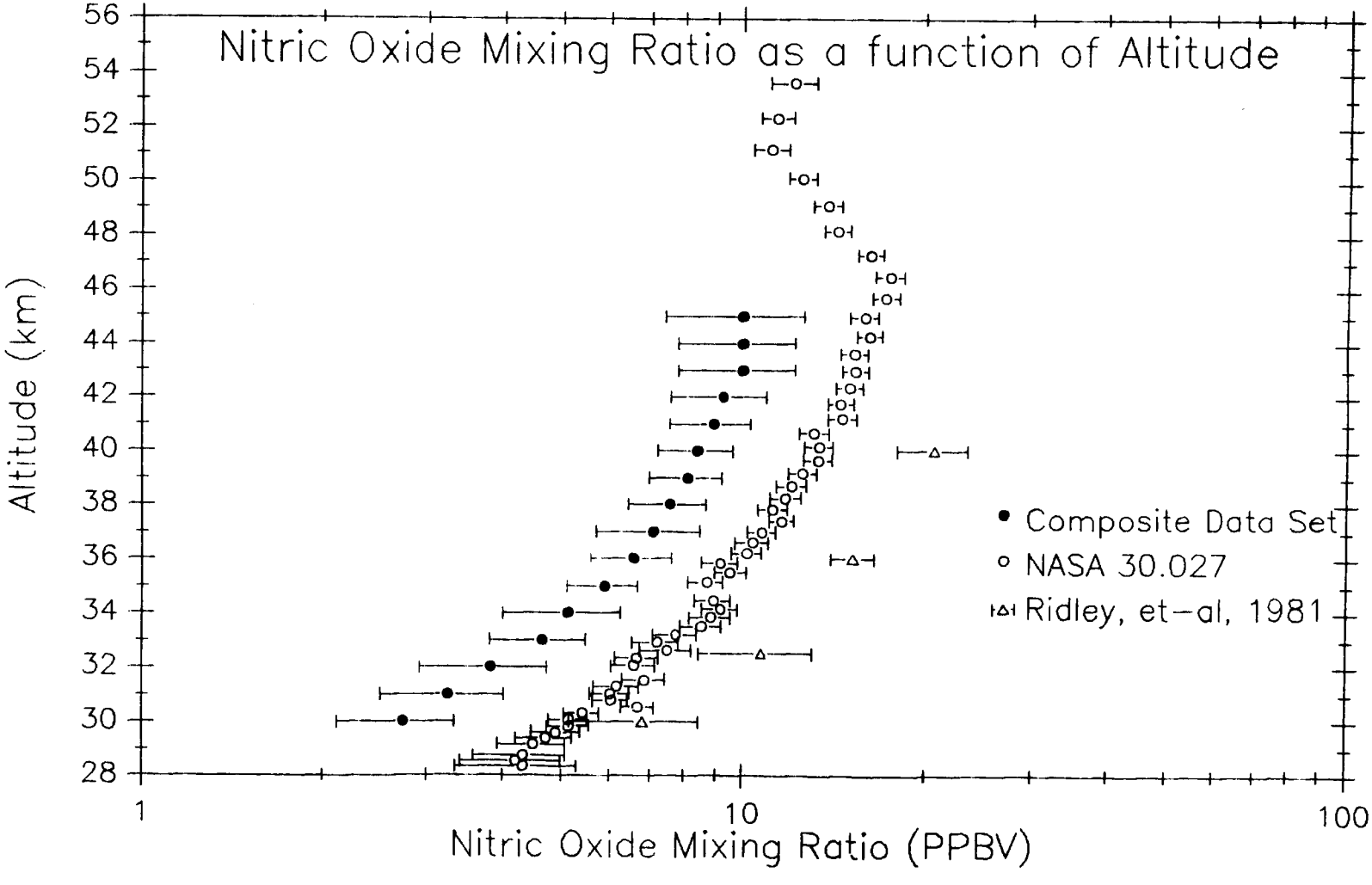
Nitric Oxide Mixing Ratio as a function of Altitude
Altitude (km)
56
54
52
50
48
46
44
42
40
38
36
34
32
30
28
1
10
100
Nitric Oxide Mixing Ratio (PPBV)
Composite Data Set
NASA 30.027
Ridley, et-al, 1981

XV. IN FLIGHT CALIBRATION

The payload flown on NASA 30.015 was instrumented with an onboard calibration gas. On parachute descent at approximately 32 km a known quantity of nitric oxide was introduced into the incomming air stream at the entrance of the inlet flow tube. The leak rate of the calibration gas was designed to be small, $0.04872cc/s$ (NTP), such that the flow rate of the incomming air stream would not be disturbed. The flow rate of the air stream through the inlet flow tube is a calibrated function of the difference pressures accross the flow tube. These pressures are continuously monitored by two Validyne pressure gauges. Table IV gives the pertinent information relating to the calibration sequence. At approx. 438 seconds of elasped time, from rocket lift-off, a solenoid valve was opened and the calibration gas was leaked into the air stream for a period of 12 seconds. The background calibration gas function was disabled during this time period. Notice that the phototube output count rate has risen to approx. 18,000 c/s. Figure 32 shows the event graphically. We fit the three levels of data to second order least squares curve fit in order separate the various signal sources. The background calibration signal contains the phototube dark count, I_B and the ozone generated background, I_o. These data are obtained every 7.0 seconds for a period of 2.0 seconds. For the purpose of this calibration measurement we have used five-2.0 second integration periods between 427 second and 470 of elapsed time. That curve fit is shown as

$$log(I_B + I_O) = 8.7518 - 2.6505E - 2 * T + 3.4503E - 5 * T^2 \tag{29}$$

Similarly we can fit a least squares curve to the output count rate signal, i.e.,

$$log(I_t) = 5.1448 - 9.2022E - 3 * T + 1.4223E - 5 * T^2 \tag{30}$$

where $I_t = I_S + I_B + I_O$ and where I_S is the signal due only to the the ambient nitric oxide.

Finally, a curve fit is obtained for the signal level due to the some of all of the signal sources, including the onboard calibration gas. This yields

$$log(I_{cal}) = -1.2402E + 1 + 7.1738E - 2 * T - 7.7057E - 5 * T^2 \tag{31}$$

In Table IV time is given at 1 second intervals and total phototube count rate is given in column I_t. Note that the background signal are grouped in pairs, the ambient signal is grouped in sets of five, at least this is the normal sequence. We are interested in the calibration sequence, specifically from 439 to 449 seconds. The data shown in the $I_B + I_O$ column is obtained from the equation above. Subtracting this background from the total signal gives the NO signal which for this case is the sum of the onboard cal gas and the ambient air. The instrument sensitivity is calculated from the instrument parameters as given in part III of this report and is shown in the column designated

$\hat{I_{NO}}$. The total nitric oxide mixing ratio can now be obtained and is given in the column, $\Omega_{(NO)*}$. These values are on the order of 43 PPBV.

The ambient air nitric oxide mixing ratio, through this calibration period was estimated by the equation for I_t, subtracting the background signal, $I_B + I_O$, and dividing by the instrument sensitivity. Finally, subtracting the ambient air mixing ratio from the total source mixing ratio gives the contribution due to the onboard calibration. This turns out to be 39.70 ± 0.76 PPBV.

Table V illustrates the magnitude of the NO mixing ratio that is due to the onboard calibration source. The ambient air sample flow is shown in column F_{NO}. The flow rate of the gas flows through a sintered stainless steel leak has been calibrated in terms of pressure. The onboard pressure gauge has been calibrated with a Solfrunt Reference gauge. Figure 33 shows the gas flow rate as a function of the calibration gas volume pressure. Based upon this pressure measurement we have determined that the flow rate was 0.04872 cc/s (NTP). Our source of NO was from Scott Specialties and the tank had an assigned mixing ratio of 10.95 PPBM. Repeated calibration testing prior to launch indicated the the loss of NO molecules within the resevoir was approx. 1 % per 3 hrs. We assigned a value of 10.8 PPBM for the flight calibration. If we refer to Table V the column labeled $\hat{\Omega_{(NO)}}$ gives the expected increased NO mixing ratio due to onboard calibration as 40.03 ± 0.19 PPBV. This is in excellent agreement with the measured value above.

Table IV

Time	I_t	$I_b + I_o$	I_s	$\hat{I_{NO}}$	$\Omega_{(NO)*}$	$\Omega_{(NO)}$	$\Omega_{(NO)\#}$
427	5341						
428	5315						
429	6686						
430	6498						
431	6637						
432	6592						
433	6773						
434	5685						
435	5525						
436	6754						
437	6843						
438	11282						
439	17312	5868	11444	262.87	43.53	4.01	39.52
440	17624	5926	11698	264.95	44.15	3.94	40.21
441	17713	5985	11728	267.03	43.92	3.88	40.04
442	17831	6045	11786	269.12	43.79	3.82	39.97
443	18262	6105	12157	271.20	44.83	3.79	41.04
444	18018	6166	11852	273.28	43.37	3.8	39.57
445	17989	6228	11761	275.36	42.71	3.81	38.90
446	18378	6290	12088	278.70	43.37	3.82	39.55
447	18864	6353	12511	282.04	44.36	3.83	40.53
448	18556	6416	12140	285.38	42.54	3.83	38.71
449	18747	6480	12267	288.72	42.49	3.83	38.66
450	13208						
451	7844						
452	7835						
453	7979						
454	7896						
455	6889						
456	6988						
457	8113						
458	8099						
459	8277						
460	8334						
461	8478						
462	7360						
463	7420						
464	8454						
465	8718						
466	8831						
467	8889						
468	9100						
469	8247						
470	8206						

ORIGINAL PAGE IS
OF POOR QUALITY

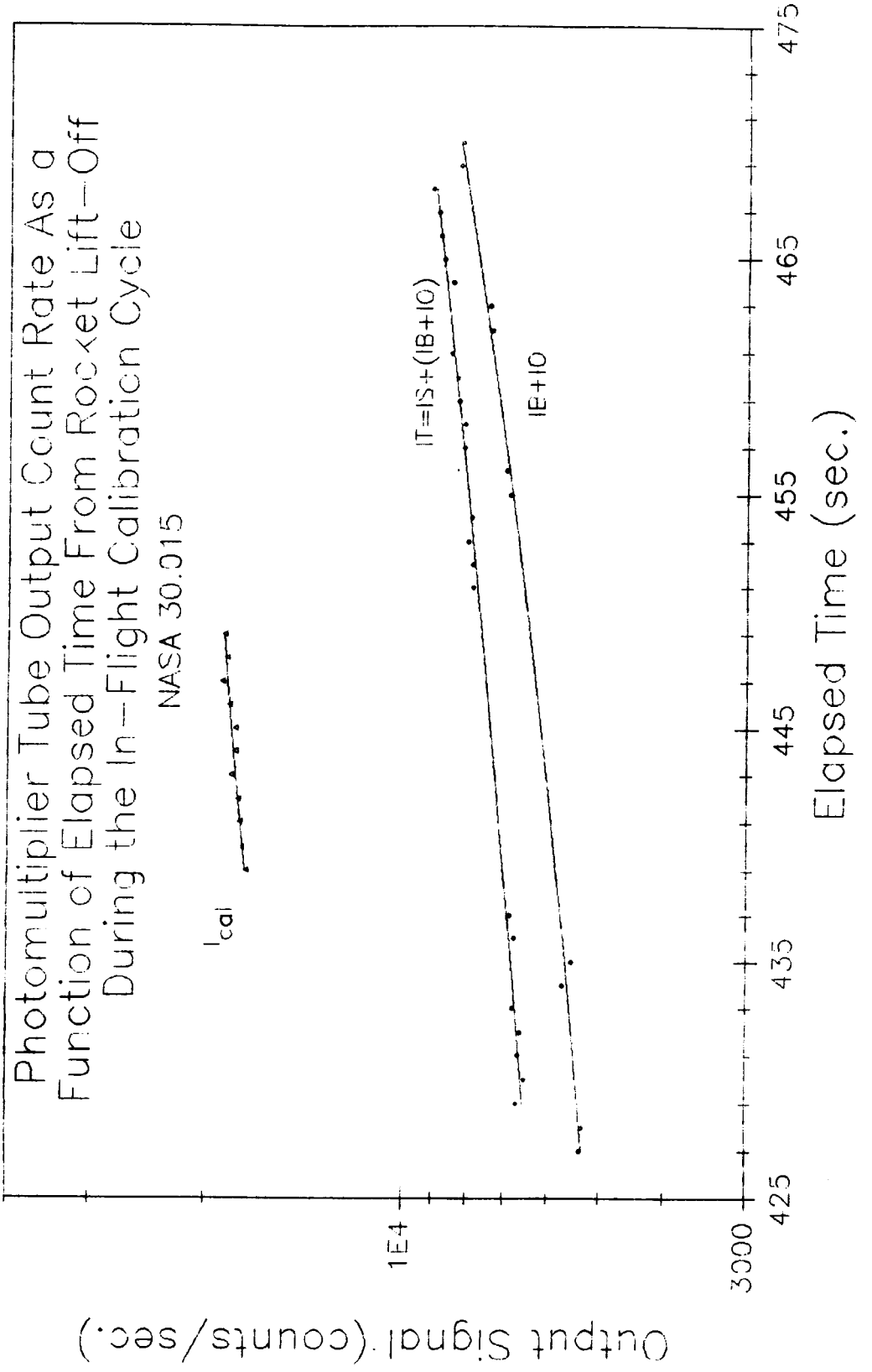

Table V

Time	F_{NO}	F_{CAL}	$\Omega_{(\dot{NO})}$
439	13.061	0.04872	40.28
440	13.087	0.04872	40.21
441	13.121	0.04872	40.10
442	13.151	0.04872	40.01
443	13.181	0.04872	39.92
444	13.207	0.04872	39.84
445	13.251	0.04872	39.71
446	13.202	0.04872	39.86
447	13.162	0.04872	39.98
448	13.052	0.04872	40.31
449	13.115	0.04872	40.12

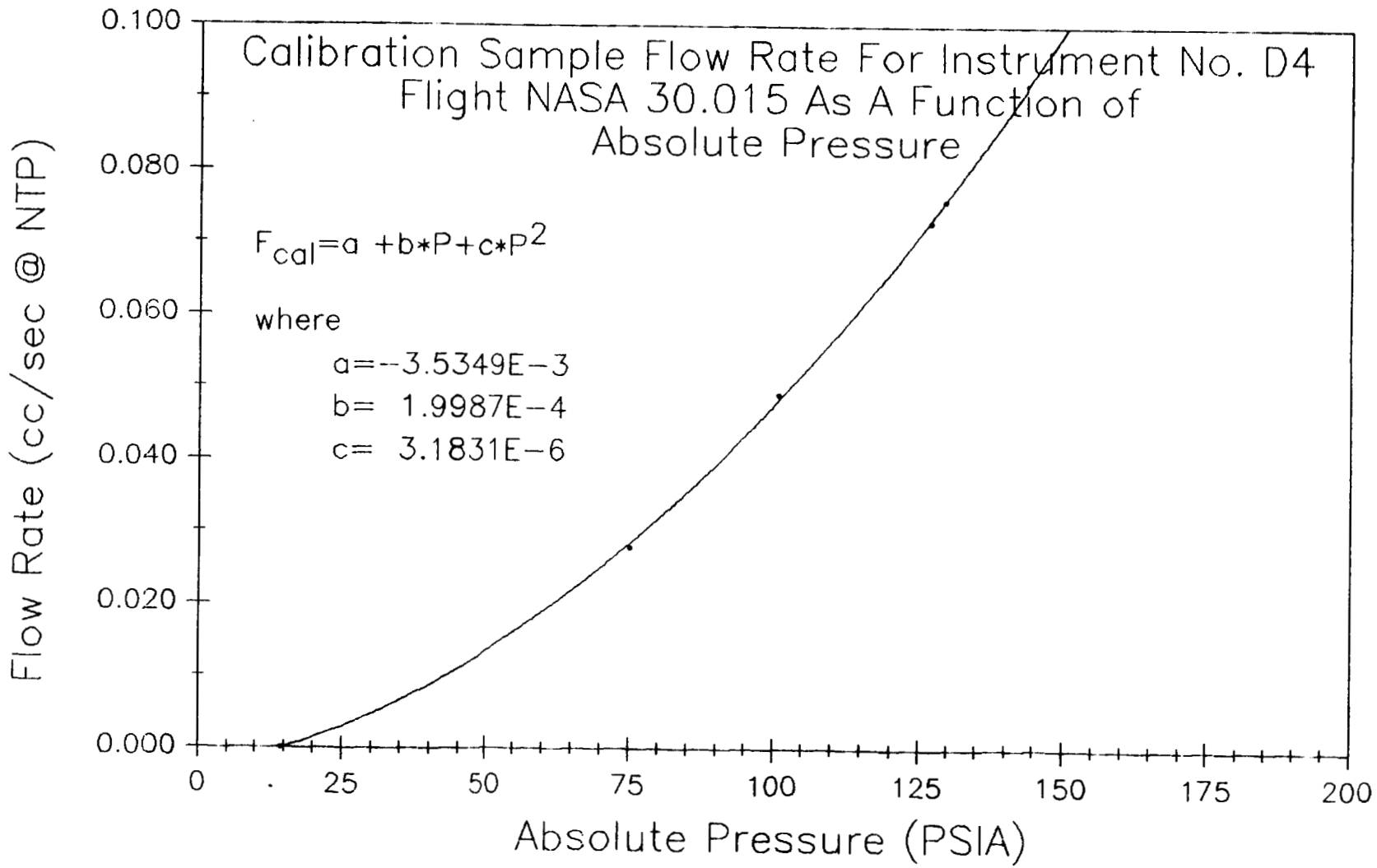
Calibration Sample Flow Rate For Instrument No. D4
Flight NASA 30.015 As A Function of
Absolute Pressure
$F_{cal}=a+b*P+c*P^2$
where
a=-3.5349E-3
b= 1.9987E-4
c= 3.1831E-6
Flow Rate (cc/sec @ NTP)
0.100
0.080
0.060
0.040
0.020
0.000
0
25
50
75
100
125
150
175
200
Absolute Pressure (PSIA)

XVI. BIBLIOGRAPHY

Ackerman, M., J. C. Fontanella, D. Frimout, A. Girard, N. Louisnard and C. Muller, Simultaneous measurements of NO and NO2 in the stratosphere, *Planet. Space Sci.*,**23**, 651, 1975.

Burkhardt, E. G., C. A. Lambert, and C. K. N. Patel, Stratospheric nitric oxide: Measurements during daytime and sunset, *Science*, **188**, 1111, 1975.

Clough, P. N., and B. A. Thrush, Mechanism of chemiluminescent reaction between nitric oxide and ozone, *Trans. Faraday Soc.*, **63**, 915, 1967.

Clyne, M. A. A., B. A. Thrust, and R. P. Wayne, *Trans. Faraday Soc.*, **60**, 359, 1964.

Drummond, J. W., J. M. Rosen and D. J. Hoffmann, Balloon-borne chemiluminescent measurement of NO to 45km., *Nature*, **265**, 319, 1977.

Evans, W. J. J., J. B. Kerr, D. T. Wardle, J. M. McConnell, B. A. Ridley, and H. I. Schiff, Intercomparison of NO, NO2, and HNO3 measurements with photochemical theory, *Can. Met. Soc.*, **14**, 189, 1976.

Evans, W. F. J., J. B. Kerr, C. T. McElroy, R. S. O'Brien, B. A. Ridley and D. I. Wardle, The odd nitrogen mixing ratio in the stratosphere, *Geophys. Res. Lett.*, **4**, 235, 1977.

Frederick, J. E., Solar corpuscular emission and neutral chemistry in the earth's middle atmosphere, *J. Geophys. Res.*, **81**, 3179, 1976.

Greaves, J. C., and D. Garvin, *J. Chem. Physics*, **30**, 348, 1959.

Horvath, J. J., and C. J. Mason, Nitric oxide mixing ratios near the stratopause measured by a rocket-borne chemiluminescent detector, *Geophys. Res. Lett.*, **5**, 1023, 1978.

Horvath, J. J., J. E. Frederick, N. Orsini and A. R. Douglass, *J. Geophys. Res.*, **88**, 10,809-10,817, 1983.

Horvath, J. J., and J. E. Frederick, In-situ measurements of nitric oxide in the high latitude upper stratosphere, *Geophys. Res Lett.*, **12** 495-497, 1985.

Johnson, H. S., and H. J. Crosby, *J. Chem. Physics*, **22**, 689, 1954.

Kays, W. M., Numerical solutions for Laminar flow heat transfer in circular tubes, *Trans. ASME*, 1265, 1955.

London, J., J. E. Frederick and G. P. Anderson, Satellite observations of the global distribution of stratospheric ozone, *J. Geophys. Res.*, **82**, 2543, 1977.

Maier, E. J., A. C. Aiken and J. E. Ainsworth, Stratospheric nitric oxide and ozone measurements using photoionization mass spectrometry and UV absorbtion, *Geophys. Res. Lett.*, **5**, 37, 1978.

Mason, C. J., A feasibility study of a rocket-borne chemiluminescent nitric oxide detector, *Space Physics Research Lab. Rpt. No. 012092-1-F, Univ. of Mich.*, 1973.

Mason, C. J., and J. J. Horvath, The direct measurement of the nitric oxide concentration in the upper atmosphere by a rocket-borne chemiluminescent detector, *Geophys. Res. Lett.*, **3**, 391, 1976.

McConnell, J. C., and M. B. McElroy, Odd nitrogen in the atmosphere, *J. Atmos. Sci.*, **30**, 1464, 1973.

Ogawa, T., and T. Shimazaki, Diurnal variations of odd nitrogen and ionic densities in the mesosphere and lower thermosphere simultaneous solutions of photochemical-diffusive equations, *J. Geophys. Res.*, **80**, 3945, 1975.

Patel, C., E. Burkhardt, and C. Lambert, Spectroscopic measurements of stratospheric nitric oxide and water vapor, *Science*, **184**, 1173, 1974.

Ridley, B. A., H. I. Schiff, A. Shaw, and J. R. Megill, In-situ measurements of stratospheric nitric oxide using a balloon-borne chemiluminescent instrument, *J. Geophys. Res.*, **80**, 1925, 1975.

Ridley, B. A., and L. C. Howlett, An instrument for nitric oxide measurements in the stratosphere, *Rev. Sci. Intr.*, **45**, 742, 1974.

Ridley, B. A., J. T. Bruin, H. T. Schiff and J. C. McConnell, Altitude profile and sunset decay measurements of stratospheric nitric oxide, *Can. Met. Soc.*, **140**, 180, 1976.

Ridley, B. A., H. I. Schiff, Stratospheric odd nitrogen: Nitric oxide measurements at 32 N in autumn, *J. Geophys. Res.*, **86**, 3167, 1981.

Stedman, D. H., T. Kelly, R. E. Shetter, J. D. Shetter and R. J. Cicerone, Feedback flow and permeation systems for the calibration of very low gas concentrations, *Air Quality Meteorology and Atmospheric Ozone, ASTM*, in press, 1978.

Wofsy, S. C., and M. B. McElroy, On vertical mixing in the upper stratosphere and low mesosphere, *J. Geophys. Res.*, **78**, 2619, 1973.